LSD1-directed therapy affects glioblastoma tumorigenicity by deregulating the protective ATF4-dependent integrated stress response

LSD1-directed therapy affects glioblastoma tumorigenicity by deregulating the protective ATF4-dependent integrated stress response

Stefania Faletti[1 †], Daniela Osti[1 †], Elena Ceccacci[1], Cristina Richichi[1], Brunella Costanza[1], Luciano Nicosia[1], Roberta Noberini[1], Giulia Marotta[1], Laura Furia[1], Mario R. Faretta[1], Silvia Brambillasca[2], Micaela Quarto[2], Luca Bertero[3], Renzo Boldorini[4], Bianca Pollo[5], Sara Gandini[1], Davide Cora[6], Saverio Minucci[1], Ciro Mercurio[2], Mario Varasi[2], Tiziana Bonaldi[1], Giuliana Pelicci[1,7 *].

[1] Department of Experimental Oncology, European Institute of Oncology (IEO), IRCCS, Milan 20139, Italy.
[2] Experimental Therapeutics Program, FIRC Institute of Molecular Oncology Foundation (IFOM), Milan 20139, Italy.
[3] Department of Medical Sciences, University of Turin, Turin 10126, Italy.
[4] Department of Health Science, University of Piemonte Orientale (UPO), Novara 28100, Italy.
[5] Unit of Neuropathology, Fondazione IRCCS Istituto Neurologico Carlo Besta, Milan 20133, Italy.
[6] Department of Translational Medicine, Center for Translational Research on Autoimmune and Allergic Disease (CAAD), University of Piemonte Orientale, Novara 28100, Italy.
[7] Department of Translational Medicine, University of Piemonte Orientale, Novara 28100, Italy.

[*]Corresponding author. Email: giuliana.pelicci@ieo.it
[†]These authors contributed equally to this work.

Abstract

Glioblastoma (GBM) is a fatal tumor whose aggressiveness, heterogeneity, poor blood-brain barrier penetration, and resistance to therapy highlight the need for new targets and clinical treatments. A step toward clinical translation includes the eradication of GBM tumor-initiating cells (TICs), responsible for GBM heterogeneity and relapse. By using patient-derived TICs and xenograft orthotopic models, we demonstrated that the selective lysine-specific histone demethylase 1 inhibitor DDP_38003 (LSD1i) is able to penetrate the brain parenchyma in vivo in preclinical models, is well tolerated, and exerts antitumor activity in molecularly different GBMs. LSD1 genetic targeting further strengthens the role of LSD1 in GBM TIC maintenance. GBM TIC plasticity supports their adaptation and survival under a plethora of environmental stresses, including nutrient deficiency and proteostasis perturbation. By mimicking these stresses in vitro, we found that LSD1 inhibition hampers the induction of the activating transcription factor 4 (ATF4), the master regulator of the integrated stress response (ISR). The resulting aberrant ISR sensitizes GBM TICs to stress-induced cell death, hampering tumor aggressiveness. Functionally, LSD1i interferes with LSD1 scaffolding function and prevents its interaction with CREBBP, a critical ATF4 activator. By disrupting the interaction between CREBBP and LSD1-ATF4 axis, LSD1 inhibition prevents GBM TICs from overcoming stress and sustaining GBM progression. The effectiveness of the LSD1 inhibition in preclinical models shown here places a strong rationale toward its clinical translation for GBM treatment.

INTRODUCTION

Glioblastoma (GBM) is the most fatal primary brain tumor in adults (*1*). Relapses occur in 80 to 90% of the cases, and despite great advances in the understanding of its pathophysiology, patient prognosis remains dismal (*1*). Current standard treatment corresponds to maximal surgical resection, followed by the combination of radiation and chemotherapy with temozolomide (*2*). However, apart from some alleviation of signs and symptoms, treatments ultimately fail because of GBM's infiltrative nature and its extensive cellular and molecular heterogeneity. GBM is composed of different cell types with different patterns of gene expression (*3*), among which are tumor-initiating cells (TICs). TICs are endowed with stem cell–like features and, in virtue of their chemoradioresistance (*4*, *5*), contribute to tumor regrowth (*6*). Stem cell–like features are not only intrinsic but also plastic properties that can be acquired and modified upon reversible state transitions. Overall, TIC plasticity and ability to adapt and survive in response to microenvironmental and therapeutic cues lay their foundation on TIC-permissive and flexible epigenetic landscape (*7*–*9*). As a consequence, therapeutic strategies targeting the molecular mechanisms supporting cellular plasticity and curb TIC-adaptive properties might eventually hinder recurrence and make GBM a more manageable disease (*7*, *8*). Gliomagenesis and stemness are both driven by genetic and epigenetic alterations. One of the best-characterized epigenetic mark is histone 3 (H3) methylation, which can activate or repress transcription depending on the specific methylated site (*10*). An increasing body of evidence points to lysine-specific demethylase 1 (LSD1; also known as KDM1A, AOF2) as a key target that may be exploited for molecular-based therapies. LSD1 demethylates mono- and dimethylated histone H3 lysine-4 (H3K4me1/2), working as a transcriptional repressor in complex with Nurd or CoREST (*11*), and histone H3 lysine-9 (H3K9me1/2), behaving as a transcriptional activator in

complex with androgen or estrogen receptor (*12*). Moreover, LSD1 demethylates nonhistone substrates (*13*). LSD1 is physiologically involved in several processes, encompassing stem cell maintenance, cell growth, and differentiation, in different cellular contexts (*14*). Its genetic ablation is embryonically lethal (*15*). In addition, LSD1 is overexpressed in different types of cancer, exerting a tumor-promoting activity (*13*, *16*). Accordingly, targeting LSD1 in GBM cells by means of gene silencing or pharmacological inhibition induces cell growth arrest, apoptotic cell death, and attenuation of stem-like cell traits (*17*–*19*). However, much remains to be elucidated about LSD1-dependent phenotype and its mechanism of action in GBM, in particular, for what concerns the TIC compartment. The tumor-promoting activity of LSD1 in different types of cancers, including GBM, has raised interest in the development of LSD1 inhibitors. LSD1 shares structural similarities with the family of monoamine oxidases (MAOs) (*11*), and several inhibitors targeting LSD1 catalytic activity derive from the MAO inhibitor tranylcypromine. Some LSD1 inhibitors have been recognized as nonselective compounds that possibly induce substantial toxicity in vitro and in vivo and make the interpretation of LSD1 role misleading (*20*). Few inhibitors are currently in clinical trials for small cell lung cancer (SCLC), lung cancer, and acute myeloid leukemia (AML) (*16*, *21*). By taking advantage of human GBM patient-derived TICs as a model system that better resembles human GBMs (*22*) and by exploiting the irreversible LSD1 inhibitor DDP_38003 (hereafter LSD1i), which already showed therapeutic benefits in mouse leukemia models (*23*, *24*), we set to address whether LSD1-directed therapy represents a new promising and reasonable treatment strategy for GBM.

RESULTS

LSD1 pharmacological inhibition has therapeutic potential prolonging the survival of GBM patient-derived xenografts

LSD1 protumorigenic role runs parallel to its overexpression in many cancer types (*13*, *16*). We confirmed that LSD1 is highly expressed in all GBM tumors analyzed (Fig. 1AOpens in image viewer and table S1), and it is overexpressed in different patient-derived molecularly heterogeneous GBM TICs in comparison with human neural progenitor cells ($P = 0.044$) (Fig. 1BOpens in image viewer and table S2). Moreover, gene expression data from the Sun and The Cancer Genome Atlas (TCGA) databases (https://cancer.gov/tcga) revealed that LSD1 is significantly enriched in human tumors in comparison with normal brain tissues (Sun dataset, $P = 0.005$; TCGA dataset, $P = 0.0000022$) (fig. S1, A and B), and its mRNA expression is up-regulated in all GBM subtypes, with proneural GBMs showing the highest expression (fig. S1C). GBM single-cell RNA sequencing (RNA-seq) data (*25*) further support that LSD1 expression is consistently higher in GBM cells with respect to matched normal cells for each of the patients analyzed (fig. S1D). Moreover, LSD1 expression spreads homogeneously within the tumor (fig. S1, E and F). Consistently, despite its variable expression among different patients, LSD1 is uniformly expressed in GBM TIC cultures. Confocal images show that all cell nuclei from the same patient with GBM TIC express LSD1 (Fig. 1COpens in image viewer). In line with this, LSD1 is equally expressed either by the putative GBM stem-like cells, defined as CD133, CD15, or Itga6-positive cells, or by the negative counterparts, all of them composing the GBM TICs in vitro (fig. S1G) (*26*).

The LSD1-specific enrichment in both GBM tissues and primary GBM TICs might help in discriminating between tumor and normal brain cells and prompted us to test the efficacy of LSD1i, an LSD1 inhibitor already characterized in terms of selectivity, efficacy, and tolerability in a murine promyelocytic leukemia model (*23*). Poor blood-brain barrier (BBB) penetration is one of the major issues responsible for drug failure in GBM therapy. For this reason, we first assessed the ability of LSD1i to penetrate mouse BBB. GBM TICs were orthotopically implanted in the nucleus caudatus of CD1-nude mice. Fourteen days after implantation, when tumor had already started to form, tumor-bearing mice were treated by oral gavage twice with LSD1i (17 mg/kg) and sacrificed 5 hours after the second administration. Through cellular thermal shift assay (CETSA) conducted on brain homogenates, we revealed a clear increase of thermodynamic stability of LSD1 in the treated group compared to the controls ($P = 0.0009$), demonstrating the ability of LSD1i to engage LSD1 inside the brain (Fig. 1DOpens in image viewer). Moreover, LSD1i treatment significantly increases H3K4me2 amount in the brains of GBM patient-derived xenografts (PDXs) ($P = 0.04$), further demonstrating the ability of LSD1i to cross the BBB and reduce LSD1 demethylase activity inside the brain (Fig. 1EOpens in image viewer). The thermal melting profile of vinculin was not affected by LSD1i (fig. S1H). To have additional indication about the tolerability of the LSD1i, we administered the inhibitor by oral gavage at the dose of 17 mg/kg, 2 days/week for 2 weeks. The treatment did not cause any sign of sufferance, modification of grooming behavior, or alterations of body weight (fig. S1I) and hematological parameters (fig. S1J). Hence, we administered LSD1i to GBM PDXs 2 days/week for 4 weeks. Treatment started 14 days after GBM TIC injection. LSD1i significantly extended mice survival compared with vehicle-treated animals ($P = 0.001$) (Fig. 1FOpens in image viewer). To gain insight into the effects of LSD1 pharmacological inhibition, subgroups of mice were sacrificed at early time points (from 1 to 4 weeks after LSD1i administration). Hematoxylin and eosin (H&E) staining revealed that only 20% of LSD1i-treated mice developed a tumor 3 weeks after treatment start, whereas 100% of control mice already developed a tumor at that time (Fig. 1GOpens in image viewer). We substantiated these results by exploiting luciferase-positive TICs derived from a different patient with GBM. CD1-nude mice were transplanted with Luc^+ GBM TICs and treated as previously described. Survival curves confirmed LSD1i therapeutic potential in terms of prolonged survival ($P < 0.0001$) (Fig. 1HOpens in image viewer). Tumor growth, monitored by bioluminescence images, was delayed in LSD1i-treated mice ($P = 0.5$) (Fig. 1IOpens in image viewer and fig. S1K). However, at the time of death and when the treatment was already finished, LSD1i-treated tumors were histologically similar to their controls (fig. S1L). The lack of temozolomide efficacy in the tested GBM TICs (fig. S1M) highlights the therapeutic efficacy of LSD1i for GBM treatment: By effectively binding LSD1 inside the brain, the compound affects GBM growth in molecularly different GBM PDXs, outperforming the standard of care.

LSD1 pharmacological inhibition reduces GBM TIC growth and self-renewal

Because human GBMs are maintained by a TIC subpopulation endowed with stem cell–related features (*6*) and LSD1 has a role in either adult, embryonic, or pluripotent stem cells (*16*), we sought to elucidate the effect of LSD1i on GBM TICs in vitro. LSD1i effectively reduced LSD1 demethylase activity in multiple GBM TICs, as demonstrated by the mild but statistically significant H3K4me2 increase (GBM#22 and GBM#11, $P < 0.05$; GBM#10 and

GBM#18, $P < 0.1$) (fig. S2A). By incubating GBM TICs once with increasing concentrations of LSD1i, we observed a clear dose-dependent reduction of cell viability. The median effective concentration (EC_{50}) values revealed that the tested GBM TICs were all sensitive to LSD1i (Fig. 1JOpens in image viewer). In contrast, LSD1i minimally affected neural progenitor cell (NPC) viability, thus strengthening the specificity of LSD1i against GBM TICs (Fig. 1JOpens in image viewer). Similar results were obtained by examining cell growth rate: LSD1i significantly reduced cell growth after 5 or 7 days of culture (GBM#22, 5 days, $P < 0.05$ and 7 days, $P < 0.01$; GBM#7 and GBM#18, 7 days, $P < 0.01$) (Fig. 1KOpens in image viewer) and affected cell survival ($P < 0.001$), as revealed by the increased caspase 3/7 activity in treated GBM TICs (Fig. 1LOpens in image viewer). In vitro, GBM TICs are functionally defined by the ability of self-renewal, for which sphere formation ability represents a surrogate. Hence, we evaluated the effect of the inhibitor on sphere formation. We found a significant reduction in sphere number in LSD1i-treated GBM TICs compared to controls (GBM#22 first plating, $P < 0.05$ and second plating, $P < 0.001$; GBM#7 second plating, $P < 0.05$; GBM#18 second plating, $P < 0.01$). This drop was more evident at the second plating, indicating that LSD1 pharmacological inhibition curtailed the subset of cells able to self-renew (Fig. 1MOpens in image viewer). LSD1i did not induce nor modify GBM TIC differentiation: No differences in the expression of putative stem cell–related (Nestin) and differentiation markers (glial fibrillary acidic protein and β-tubulin) were measured (fig. S2B). These results indicate that the compound inhibits LSD1 enzymatic activity and is effective in reducing both cell viability and stemness in vitro independently of GBM TIC molecular profile.

LSD1 genetic targeting mirrors LSD1 pharmacological inhibition in GBM TICs

To validate the specificity of the phenotype obtained by LSD1 pharmacological inhibition, we genetically abrogated LSD1 expression in GBM TICs by either CRISPR-Cas9 or lentiviral silencing. Two different LSD1-KO (knockout) clones derived from the same GBM#22 patient (hereby, LSD1-KO#1 and LSD1-KO#2) were generated. These cells showed reduced growth (KO#1, $P < 0.01$ and KO#2, $P < 0.001$) (Fig. 2AOpens in image viewer) and impaired self-renewal ($P < 0.001$) (Fig. 2BOpens in image viewer). LSD1 deletion compromised GBM TIC tumorigenic potential. The life span of mice orthotopically injected with LSD1-KO#1 cells significantly increased relative to controls ($P = 0.001$). By day 50 after tumor induction, all control mice have been sacrificed at the appearance of neurological signs, whereas mice transplanted with LSD1-KO#1 cells survived longer (Fig. 2COpens in image viewer). LSD1-KO#2 cells completely lost their tumorigenicity (Fig. 2COpens in image viewer). Moreover, the injection of LSD1-KO#1 and control GBM TICs in limiting dilution conditions demonstrated that LSD1 deletion significantly reduced the stem cell content ($P = 0.000142$) (Fig. 2DOpens in image viewer). However, at the time of death, LSD1-KO#1 GBM PDXs were similar to their controls (fig. S3A). These phenotypes were recapitulated by exploiting LSD1-silenced GBM TICs. LSD1-silenced cells (sh71) showed a reduced in vitro growth compared to their controls (shNT) (Fig. 2EOpens in image viewer), mainly due to their increased cell death (GBM#22, $P < 0.05$; GBM#7, $P < 0.001$) (Fig. 2FOpens in image viewer). Furthermore, LSD1 silencing significantly reduced GBM TIC self-renewal ability (GBM#22, $P < 0.05$; GBM#18 and GBM#10, $P < 0.001$) (Fig. 2GOpens in image viewer) and stem cell content ($P < 0.0001$) (Fig. 2HOpens in image viewer), measured by either sphere formation or limiting dilution in vitro assays, respectively. In vivo, LSD1 silencing significantly prolonged the life span of tumor-bearing mice relative to controls (GBM#22, $P < 0.005$; GBM#18, $P < 0.001$)

(Fig. 2IOpens in image viewer) and lowered the stem cell content ($P < 0.0001$) (Fig. 2JOpens in image viewer). To study the impact of LSD1 knockdown on GBM initiation, we sacrificed the mice at an early time point before the onset of neurological signs (4 weeks after GBM TIC injection): 66% of control mice developed large tumors, whereas LSD1-silenced tumors were still undetectable by H&E staining at that timing (fig. S3B). LSD1-silenced tumors started to appear later after intracranial injection, and at the time of death, they expressed *LSD1* mRNA and protein amount comparable to controls [not significant (n.s.)] (fig. S3, C and D). This might suggest that LSD1-silenced cells have been counterselected to allow tumor growth. Overall, these results demonstrate that LSD1 expression is critical to tumor growth, and its genetic abrogation strongly reduces viability, stemness, and tumor-forming potential in multiple patient-derived GBM TICs, thus resembling the phenotype induced by LSD1i.

LSD1 targeting affects ATF4-mediated ISR in GBM TICs

To dissect the molecular mechanisms through which LSD1 sustains GBM TIC tumorigenic properties, we performed a global transcriptomic profiling (RNA-seq) in LSD1-silenced (sh71) and control (shNT) GBM#22 TICs. The differential expression analysis yielded a short list (n = 48) of differentially expressed genes (DEGs) [$|\log_2 FC| > 1.2$ and false discovery rate (FDR) ≤ 0.05]. Nearly all of them were down-regulated upon LSD1 silencing (Fig. 3AOpens in image viewer). Gene ontology (GO) analysis revealed that these DEGs were enriched in responses to endoplasmic reticulum (ER) stress, the unfolded protein response (UPR), and nutrient deprivation (Fig. 3BOpens in image viewer). Results of gene set enrichment analysis (GSEA) further confirmed these findings, highlighting that LSD1 silencing negatively regulates the expression of genes involved in response to unfolded/misfolded proteins and amino acid metabolism (Fig. 3COpens in image viewer). Such stresses, together with different others, are known to activate an adaptive program known as integrated stress response (ISR), with the final aim to allow the cells to recover and restore homeostasis (*27*). The ISR-initiating signals converge in the activation of a common hub, the activating transcription factor 4 (ATF4) (*27*). Ingenuity Pathway Analysis revealed that ATF4 was one of the upstream regulators predicted as significantly inhibited in our model system ($P < 5.15 \times 10^{-15}$) (Fig. 3DOpens in image viewer). Accordingly, the ER stress response to tunicamycin was predicted to be inhibited as well (Fig. 3DOpens in image viewer), whereas the human homolog of *Drosophila* tribbles (TRIB3)–dependent response was activated in accordance with the decreased cell survival and increased cell death measured upon LSD1 targeting (Fig. 3DOpens in image viewer). TRIB3 is known to be involved in the control of cell death (*28*) and in the regulation of the ISR by a negative feedback mechanism (*29*). A significant reduction of ATF4 mRNA expression was measured in either LSD1-silenced (GBM#22 and GBM#18, $P < 0.01$; GBM#7, $P < 0.05$; GBM#10, $P < 0.001$) (Fig. 3EOpens in image viewer) and LSD1-KO GBM TICs ($P < 0.05$) (fig. S4A). This down-regulation was measured in TICs isolated from different patients with GBM (Fig. 3EOpens in image viewer). As a confirmation, control and LSD1-silenced GBM TICs were transduced with a lentiviral reporter vector in which green fluorescent protein (GFP) expression reflects *ATF4* promoter activity (*30*). As assessed by fluorescence-activated cell sorting (FACS) analysis, the GFP expression was strongly decreased by LSD1 silencing (Fig. 3FOpens in image viewer). To test whether LSD1 was necessary for the expression and induction of ATF4 in GBM TICs, we forced ATF4 activation by treating cells with thapsigargin and l-histidinol, two known inducers of ER and nutrient

stress, respectively (*31*, *32*). Under these conditions, PERK and GCN2 kinases trigger the phosphorylation of eIF2a (*27*), thereby inhibiting its function and abolishing general translation. Concurrently, eIF2α phosphorylation increases the expression of ATF4 (*27*), which promotes the transcription of its effector genes with the final aim to restore cell homeostasis. Stress-induced ATF4 is mainly regulated at the protein level (*27*). Under nonstressed conditions, p-eIF2a and ATF4 proteins were nearly undetectable in GBM TICs (Fig. 3, G and HOpens in image viewer). Upon thapsigargin treatment, both control (shNT-GBM#22) and LSD1-silenced (sh71-GBM#22) cells responded by increasing the phosphorylation of eIF2a, which, in turn, resulted in up-regulated ATF4 protein (Fig. 3GOpens in image viewer). ATF4 up-regulation was remarkably reduced upon LSD1 silencing (P = 0.01), whereas the amount of both eIF2 phosphorylation and total eIF2a was not affected (n.s.) (Fig. 3GOpens in image viewer). Similar results were obtained upon l-histidinol treatment (P = 0.00029) (Fig. 3HOpens in image viewer). Consistent with the results obtained in LSD1-silenced GBM TICs, LSD1-KO diminished ATF4 protein induction (P = 0.044) without affecting the amount of both p-eEIF2a and total eIF2a (n.s.) (fig. S4B). ATF4 regulates the expression of many genes involved in cell metabolism, amino acid transport, and resistance to oxidative stress in different cell types (*33*). Some of the deregulated genes identified in the RNA-seq are known ATF4 downstream genes and belong to these categories (*ASNS*, *CHAC1*, *DDIT3/CHOP*, *GDF15*, *NARS*, *PSAT1*, *SLC7A11*, *TRIB3*, and *XPOT*). We confirmed their down-regulation and that of other known ATF4 target genes by quantitative reverse transcription polymerase chain reaction (qRT-PCR) in either different LSD1-silenced (Fig. 3IOpens in image viewer and fig. S4, C and D) or LSD1-KO GBM TICs (fig. S4E). Overall, these findings suggest that LSD1 drives the expression of either ATF4 or its target genes in GBM TICs independently from eIF2a phosphorylation. Ectopic LSD1 expression (ΔN-LSD1^{WT}) in LSD1-KO GBM TICs (Fig. 4AOpens in image viewer) increased cell growth (Fig. 4BOpens in image viewer) and sphere-forming potential (Fig. 4COpens in image viewer) in comparison to mock-transduced LSD1-KO TICs. Likewise, ATF4 protein was augmented (P = 0.028) (Fig. 4AOpens in image viewer). Similarly, ATF4 overexpression in LSD1-silenced GBM TICs (Fig. 4DOpens in image viewer) rescued cell growth (Fig. 4EOpens in image viewer), mitigated cell death (Fig. 4FOpens in image viewer), and partially rescued sphere formation ability (Fig. 4GOpens in image viewer). Moreover, ATF4 overexpression specifically rescued the expression of some of its downstream genes (Fig. 4, D and HOpens in image viewer). Consistent with LSD1 genetic targeting results, LSD1i treatment slowed down ATF4 protein induction in response to either thapsigargin or l-histidinol. In control cells, ATF4 expression reached a peak 3 hours upon thapsigargin or l-histidinol treatment and dropped at 6 and 24 hours, indicating that the cells were solving the stress. Conversely, ATF4 induction in LSD1i-treated GBM TICs was weaker and prolonged, being maintained for up to 24 hours (thapsigargin, P = 0.044; l-histidinol, P = 0.031) (Fig. 5, A and BOpens in image viewer). We further confirmed these results by triggering ER stress with tunicamycin. LSD1i treatment reduced the tunicamycin-dependent ATF4 induction at the early time points (3 and 6 hours) but prolonged ATF4 expression (24 hours) once the control cells solved the stress (P = 0.029) (Fig. 5COpens in image viewer). Irrespective of the stimuli used, no modulation of either eIF2a phosphorylation or total eIF2a was observed upon LSD1i treatment (n.s.) (Fig. 5, A to COpens in image viewer). Similar results were obtained with GBM TICs from different patients and in response to different stressors (GBM#7, P = 0.024; GBM#10, P = 0.03; GBM#18, P = 0.01) (fig. S5, A to C). Accordingly, the induction of ATF4 target genes involved in response to stress, rapid and transient in controls, persisted in

LSD1i-treated GBM#22 (Fig. 5DOpens in image viewer) and GBM#7 (fig. S5D) TICs upon l-histidinol treatment. The brief ATF4 protein induction supported the growth of control GBM TICs experiencing ER stress or nutrient deprivation (Fig. 5EOpens in image viewer and fig. S5E). Conversely, LSD1i-treated cells were more sensitive to either thapsigargin or l-histidinol (Fig. 5EOpens in image viewer and fig. S5E). We measured a synergistic cooperation between LSD1i and either l-histidinol (excess over Bliss score, GBM#22 TICs: 13; GBM#7 TICs: 14) or thapsigargin (excess over Bliss score, GBM#22 TICs: 13) in diminishing GBM TIC growth (Fig. 5EOpens in image viewer and fig. S5E). Likewise, when nutrient stress was induced by glutamine withdrawal, LSD1 inhibition restricted ATF4 induction ($P = 0.005$) (fig. S5F) and synergized with glutamine depletion to reduce in vitro growth of GBM TICs (excess over Bliss score, GBM#22 TICs: 15) (Fig. 5FOpens in image viewer). Overall, these results suggest that LSD1 pharmacological inhibition impairs the ability of GBM TICs to promptly and properly activate the ISR, resulting in the prolonged activation of the ISR, which affects GBM TIC survival under different stress conditions.

LSD1 and ATF4 share common DNA binding sites

By exploiting chromatin immunoprecipitation (ChIP) followed by next-generation sequencing (ChIP-seq), we profiled LSD1 genome-wide binding on GBM TIC genome. A total of 50,967 LSD1 peaks were identified ($P < 10^{-10}$). A total of 25.76% of LSD1 binding sites were distributed over promoter regions. Specifically, 18.93% lie within the 1–kilo–base pair (kbp) region surrounding the transcription start site (TSS) (fig. S6A). Distal intergenic and intronic regions were occupied by 30.26 and 29.85% of LSD1 peaks, respectively (fig. S6A). The broad LSD1 binding in the genome is in agreement with results from other cellular models (*34*). LSD1 bound the promoters of nearly all its DEGs ($n = 44$ of 48) (Fig. 6AOpens in image viewer). We confirmed these results independently by ChIP followed by qPCR of candidate genes (ChIP-qPCR) (Fig. 6BOpens in image viewer). As previously reported, most of these DEGs are known ATF4 downstream effectors. We found that a previously recognized computationally predicted ATF4-binding motif was significantly enriched among LSD1-bound DEGs (empirical $P = 0.032$) (Fig. 6COpens in image viewer). To further link LSD1 and ATF4, we demonstrated by ChIP-qPCR that LSD1 was able to bind the *ATF4* promoter itself (Fig. 6DOpens in image viewer), and in turn, ATF4 bound LSD1 target genes in the same region already occupied by LSD1 (Fig. 6EOpens in image viewer). An in silico analysis of LSD1 and ATF4 ChIP-seq data in myeloid leukemia K562 cells demonstrated the overlap of LSD1 and ATF4 around promoter regions of protein-coding genes ($P < 10^{-188}$) (fig. S6B). The fact that LSD1 and ATF4 share the binding site inside the promoter of LSD1 target genes suggests that they might cooperate to regulate their expression.

Many of the available LSD1 inhibitors displace LSD1 from its targets genes (*24*, *34*, *35*). Thus, we verified whether LSD1i was able to modify LSD1 binding profile as well. Genomic annotation of LSD1 binding sites was unchanged by LSD1i treatment (fig. S6C), indicating that LSD1i did not modify the genome-wide distribution of LSD1. We classified LSD1-bound regions as “common” if conserved independently by LSD1i, “gain” if present only in LSD1i-treated cells, and “lost” if present only in vehicle-treated cells. Out of 50,967 LSD1 peaks, 30,924 have been identified as common regions, 5432 as gain, and 10,266 as lost regions (Fig. 6FOpens in image viewer). Model-based analysis of Chip-seq (MACS) scores of peaks within common regions were higher than those in gain and lost regions (fig. S6D), and promoter regions were mainly included in the common regions (fig. S6E). A site-specific

analysis confirmed that LSD1 maintained the binding at the promoter region of its 44 DEGs upon LSD1i treatment (Fig. 6, G and HOpens in image viewer, and fig. S6F). ATF4 binding to the promoter of its target genes was not modified by LSD1 pharmacological inhibition (Fig. 6IOpens in image viewer).

Mechanistically, we tested whether LSD1 demethylase activity was required for the regulation of LSD1 target genes. ChIP-seq experiments demonstrated that LSD1i treatment increased H3K4me2 (vehicle median, 1.25; LSD1i median, 4.03; P = 0e +00) and, to a lesser extent, H3K4me3 amount (vehicle median, 1.26; LSD1i median, 2.54; P = 0e +00), in the common regions, whereas H3K4me1 was unchanged (fig. S6G). H3K4 methylation in gain and lost regions was not modified by LSD1i (fig. S6G). In accordance, LSD1i significantly increased H3K4me2 amount at the promoters of the LSD1-bound DEGs (vehicle mean, 1.45; LSD1i mean, 3.81; Bonferroni-corrected P= 0.001) (fig. S6H). The enrichment of H3K4me2 due to the inhibition of LSD1 catalytic activity was not directly associated with the change in gene expression or chromatin accessibility, as assessed by RNA-seq and assay for transposase-accessible chromatin sequencing (ATAC-seq), respectively (fig. S6I). To further assess the role of LSD1 catalytic activity, we transduced LSD1-KO GBM TICs with either wild-type (WT) (Δ*N-LSD1*^{WT}) or catalytic mutant LSD1 complementary DNA (cDNA) (Δ*N-LSD1*^{K661A}) (Fig. 6JOpens in image viewer). Ectopic expression of WT and mutant LSD1 in KO cells significantly increased cell growth (Δ*N-LSD1*^{WT}, $P < 0.05$; Δ*N-LSD1*^{K661A}, $P < 0.01$) (Fig. 6KOpens in image viewer) and self-renewal ability ($P < 0.05$) (Fig. 6LOpens in image viewer) compared to mock-transduced cells. Moreover, they equally increased ATF4 mRNA (Fig. 6MOpens in image viewer) and protein (P = 0.01) (Fig. 6JOpens in image viewer), as well as the mRNA of the ATF4 effector *ASNS* (Fig. 6MOpens in image viewer). Together, these results demonstrate that LSD1 demethylase activity was not required to rescue the phenotype induced by LSD1 depletion.

LSD1i treatment reduces ATF4 activation by modifying LSD1 protein complex in GBM TICs

Given the fact that LSD1 physically interacts with several proteins and transcription factors (*36*), we next investigated whether LSD1i could lead to the disruption of protein-protein interaction within LSD1 protein complex, thus accounting for the above-described results. We first characterized the basal LSD1 interaction network in GBM#22 TICs using mass spectrometry (MS) approach [tandem MS (MS/MS)]. To discriminate the specific LSD1 interactors, we performed LSD1 coimmunoprecipitation (co-IP) in the presence of an excess fold of the soluble LSD1-blocking peptide (fig. S7A). We identified 360 proteins as putative LSD1 interactors, which included both proteins reproducibly detected only in the LSD1-IP and enriched in this fraction compared to the mock control (table S3). By interrogating g:Profiler (https://biit.cs.ut.ee/gprofiler/gost) and CORUM database (http://mips.helmholtz-muenchen.de/corum/), we found that LSD1 interactors were enriched in the best-known complexes CoREST, CtBP, and BHC complexes (Fig. 7AOpens in image viewer) (*36*). Several complexes associated with H3K4 methyltransferase activity, such as the MLL3, the MLL4, and the PTIP-HMT complexes (*37*), were enriched as well (Fig. 7AOpens in image viewer). A further analysis with ClueGO (https://apps.cytoscape.org/apps/cluego) revealed that the proteins coimmunoprecipitated with LSD1 were mostly involved in chromosome organization, histone PTM activity, regulation of transcription, and DNA repair (fig. S7B). Upon treatment with LSD1i, nuclear proteins co-IP with LSD1 in control and LSD1i-treated GBM#22 TICs were analyzed through MS/MS, and LSD1 protein interactors were classified

on the basis of their label-free quantitation values as follows: (i) proteins that remained stably associated to LSD1 in the presence of the inhibitor; (ii) proteins whose abundance within the LSD1 co-IP increased after LSD1 inhibition, defined as "recruited"; and (ii) proteins whose abundance decreased in the LSD1 co-IP in the presence of the drug, defined as "evicted." Overall, most of the interactors remained stably associated with LSD1 upon LSD1i treatment (Fig. 7BOpens in image viewer and table S3). Among the few proteins that lost their association after treatment with LSD1i, we focused on CREBBP [also known as cyclic adenosine monophosphate response element–binding protein (CREB)–binding protein (CBP)], given its role as transcriptional coactivator of many different transcription factors (*38*). ATF4 contains a bZIP domain that directly interacts with p300/CBP (*39*). In turn, CBP and p300 are able to acetylate ATF4 in that domain, thus enhancing its transcriptional activity (*40*). The STRING database (https://string-db.org/) predicted the interaction between LSD1, CBP, and ATF4 in GBM TICs (fig. S7C). An in silico analysis on TCGA revealed a strong positive correlation between LSD1 and CBP expression in patients with GBM, further supporting our results (fig. S7D). We confirmed LSD1 and CBP interaction using proximity ligation assay (PLA) in GBM#22 TICs, GBM#23 TICs (Fig. 7COpens in image viewer and fig. S7E), and in MCF10A normal breast cells (fig. S7F). LSD1i did not affect CBP expression, therefore strengthening its eviction from LSD1 protein complex (fig. S7, G and H). Together, these results led us to hypothesize that LSD1 regulates ATF4-dependent transcription as part of a complex that includes CBP; by forcing CBP out from this complex, LSD1i impairs ATF4 transactivation. GBM TICs with reduced CBP expression ($P = 2.05 \times 10^{-6}$) (Fig. 7DOpens in image viewer, left) failed to respond to l-histidinol–induced nutrient stress as measured by impaired induction of both ATF4 ($P = 0.03$) (Fig. 7DOpens in image viewer, right) and ATF4 target genes (Fig. 7EOpens in image viewer), confirming CBP as a positive regulator of the ISR activation in GBM TICs. We then assessed the role of CBP as a mediator of LSD1i by evaluating the effect of LSD1i treatment upon CBP knockdown. In the absence of stress (basal), CBP silencing (shCBP + vehicle) showed a limited effect on the growth of GBM#22 TICs compared to control cells (Crtl + vehicle). Upon l-histidinol treatment, CBP knockdown reduced the growth of GBM#22 TICs (Fig. 7FOpens in image viewer). Both in basal and l-histidinol–treated cells, LSD1i efficiently reduced the growth of control GBM#22 TICs, whereas its effect on CBP-silenced cells was less detrimental (Fig. 7FOpens in image viewer), revealing an antagonism between LSD1i and CBP knockdown (excess over Bliss score, −13 and −6, respectively). In line with this phenotype, LSD1i induced a prolonged transactivation of ATF4 downstream effector genes in stressed control GBM#22 TICs but not in CBP-silenced ones (Fig. 7GOpens in image viewer). Together, these data show that the efficacy of LSD1i is hampered by CBP knockdown, thus strengthening the role of CBP as a critical mediator of LSD1-ATF4 signaling axis in the regulation of GBM TIC stress response.

DISCUSSION

In the present study, we show that LSD1 might be a therapeutically relevant target in human GBM. In line with its role in normal and cancer stem cells and its tumor-promoting activity in different malignancies (*13*, *16*), LSD1 enrichment in human and mouse models of GBMs as well as in patient-derived primary TICs led us to demonstrate that LSD1 inhibition effectively impairs the tumor-initiating potentials in GBM. Being at the apex of GBM hierarchy, TICs are responsible for either GBM onset, regrowth, or extensive heterogeneity (*6*). The direct consequence of GBM TIC persistence beyond any therapeutic approach is the inevitable and

rapid relapse of this continuously evolving tumor, eventually culminating in patient death. Thus, targeting GBM TIC population and inhibiting the mechanisms that sustain GBM cell plasticity are likely necessary to completely eradicate GBM. The dysregulated expression of LSD1 and other different histone modifiers and epigenetic effectors is common in cancer. This is why molecules targeting epigenetic traits are currently evaluated in preclinical and clinical trials (*41*). In the case of GBM, histone deacetylase inhibitors have been tested both as monotherapy and in combination in several ongoing clinical trials (*42*). As far as LSD1 inhibitors, some of them already progressed to human clinical trials for treatment of SCLC, lung cancer, and AML but, at the best of our knowledge, not for GBM (*16*, *21*). In this study, we demonstrate that LSD1 is an effective target in GBM by using both pharmacologic and genetic targeting. The selective, irreversible, orally bioavailable, and brain-penetrant LSD1i DDP_38003 exerts antitumor effects in preclinical models in vitro and in vivo against GBM TICs obtained from different patients and in a manner independent of their molecular profiles. LSD1i treatment reduced GBM TIC growth, blocked stemness, and delayed tumor onset and growth in GBM PDX models. Of note, LSD1i treatment did not exert any evident sign of toxicity, suggesting the existence of a therapeutic window for its administration. Further support to LSD1i efficacy comes from its application in hematological malignancies, either alone (*23*) or in combination with retinoic acid (*24*). LSD1 silencing and KO in GBM TICs phenocopied LSD1i effects. Other studies demonstrated LSD1 enrichment in GBM TICs compared with normal progenitor cells, as well as the sensitivity of GBM TICs toward LSD1 inhibitors, despite the inhibitors used in the studies being more active on MAOs than on LSD1 (*18*, *43*, *44*). The genes found to be deregulated upon LSD1 silencing suggested an association with the ISR in GBM TICs. The ISR is an adaptation pathway critical for cell survival under different stresses: Once the stress is solved, ISR activation decreases. However, its prolonged activation can trigger cell death (*27*). The ISR mediates its effects by reducing global protein synthesis while inducing ATF4 expression, which, in turn, coordinates the adaptive response in cells. ATF4 effectors are involved in different processes including cell metabolism, amino acid synthesis and transport, resistance to oxidative stress, stem cell maintenance and differentiation, proliferation and survival, invasive tumor growth, and angiogenesis (*33*, *45*). Given the high proliferation index, GBM cells are able to divide despite the lack of nutrients and oxygen and the accumulation of unfolded proteins. LSD1 genetic targeting reduces ATF4 expression under nonstressed conditions and prevents ATF4 induction upon either ER or nutrient stress. Likewise, LSD1 pharmacological inhibition impairs the ability of GBM TICs to promptly and properly solve the ISR. LSD1i first limits ATF4 induction upon stress and then prolongs its activation, leading to the death of cells experiencing stress. LSD1i protracts the transcription of proapoptotic mediators. Among these are *TRIB3*, known to be implicated in ATF4-mediated cell death (*28*); *CHAC1*, whose overexpression has been associated to enhanced apoptosis (*46*); and *DDIT3*, directly involved in the UPR-induced cell death pathway (*47*). The persistent induction of ATF4 and DDIT3 promotes apoptosis in GBM cells in response to ER stress (*19*). Among the genes whose expression persists in LSD1i-treated cells is *ATF3*, a member of the ATF/CREB family of transcription factors. ATF3 and ATF4 form a complex that enhances *DDIT3* transcription to induce apoptosis (*48*). Upon ER stress, ATF3 was reported to bind to *AP-1* motif-enriched DNA traits and inhibit pivotal oncogenic pathways, including extracellular signal–regulated kinase/mitogen-activated protein kinase signaling (*49*). Likewise, NPCs exert an antitumorigenic effect in WHO grade III and grade IV astrocytomas by inducing a prolonged ATF3-mediated ER stress response in tumor cells, which leads to

their apoptosis (*50*). LSD1 activity has already been associated with UPR, ER stress pathway, and oxidative stress response in GBM TICs. However, in this work, LSD1 inhibitors themselves were able to activate the UPR pathway, concomitantly triggering differentiation and apoptosis (*19*). Our results indicate that LSD1 signals on ATF4 independently from eIF2a phosphorylation. In addition to translational control, ATF4 expression might be subject also to transcriptional regulation (*51*). In GBM TICs, LSD1 knockdown/KO reduces the mRNA of *ATF4* and *ATF4* target genes in an LSD1-dependent fashion. LSD1 directly binds ATF4 promoter and shares with ATF4 the binding sites of well-known ATF4 effectors. It is thus conceivable that LSD1 and ATF4 cooperate to regulate the expression of their common target genes. In agreement with this, KDM4C, another member of the KDM family, cooperates with ATF4 in neuroblastoma for the transcriptional activation of serine pathway genes for cancer cell proliferation (*52*). ATF4 is highly expressed and sustains tumorigenicity in different cancers, including GBM (*45*, *51*), and different oncogenes signal on it (*52–54*). Moreover, ATF4 associates with poorer patient overall survival, including that of patients with GBM (*45*, *55*). Collectively, these findings strengthen the link between LSD1 and ATF4 in supporting GBM formation likely through the tight coordination of the transcriptional response of GBM TICs to stress. In agreement with this, the reconstitution of ATF4 expression in LSD1-KO GBM TICs was able to restore the growth and stemness of GBM TICs, together with the expression of some ATF4 target genes. LSD1 is a component of different multiprotein complexes, and the mechanism mediating its tumor-promoting activity might rely on either its enzymatic activity or its scaffolding role. Recent evidences highlight the involvement of the demethylase-independent function of LSD1 in cancer progression (*24*, *34*, *35*, *56*, *57*). Here, the convergence of LSD1 genetic and pharmacological targeting phenotypes supports the scaffolding function of LSD1, rather than its histone demethylase activity, in sustaining GBM TIC growth and survival through the ATF4-dependent ISR. The inhibitor did not affect chromatin occupancy of either LSD1 or ATF4 at select genes, and albeit H3K4me1/me2 amount increased in correspondence to LSD1 binding sites, this was not linked to changes in gene expression. Moreover, the expression of either the WT or the enzymatic-deficient human mutant protein $LSD1^{K661A}$ in LSD1-KO GBM TICs equally rescued growth and stemness and restored ATF4 expression. The catalytically inactive $LSD1^{K661A}$ does not exert H3K4 demethylase activity on histone H3 peptide or protein substrates (*58*). Albeit a residual H3K4 demethylase activity was measured on nucleosomes only recently (*59*), the efficiency of K661A mutation in impairing many LSD1 functions has been described (*60*, *61*). However, given the high number of proteins other than histones that have been identified as substrates of LSD1 catalytic activity, we cannot rule out any effects due to LSD1 nonhistone protein demethylation. MS results showed that, among the interactors in GBM TICs, LSD1 binds CBP. CBP is a crucial mediator of stress-dependent ATF4 induction: It directly binds ATF4 (*39*) and enhances ATF4 transcriptional activity (*40*). Of interest, proteomic results and confocal PLA images demonstrate LSD1 and CBP interaction in the GBM context. Moreover, being reproducible also in human normal breast cells, it is conceivable that this interaction is part of a general mechanism of ATF4 regulation. In GBM TICs, LSD1i treatment modified LSD1 protein complex by displacing CBP, eventually preventing ATF4 induction. Consistently, CBP silencing not only mirrored LSD1 inhibition hampering a proper ISR activation but also antagonized the efficacy of LSD1i itself. This bolsters the role of CBP as a mediator of LSD1i-dependent phenotype. In line with our findings is the very recent demonstration that CBP promotes GBM TIC maintenance and GBM growth as part of a regulatory complex activating downstream gene transcription (*62*).

Our study raises some questions. Although LSD1-specific enrichment in GBMs likely discriminates between tumor landscape and normal brain, thus providing the basis for clinical studies using LSD1 inhibitors for brain tumor management, LSD1's wide expression throughout the body and its crucial role in different physiological processes need a deeper characterization of LSD1-directed therapy in clinical setting. In addition, the use of immunocompromised mice bearing human GBM limits our ability to fully characterize the interaction between GBM cells and the inflammatory environment. Detailed experiments and safety studies in larger animals will better define the clinical translatability of LSD1i. Moreover, we are aware that, given the high heterogeneity of human GBMs, the clinical validation of our results would benefit from testing a larger cohort of patients. In conclusion, our results have identified a direct association between LSD1-CBP-ATF4 signaling axis and the ISR, highlighting the role of LSD1 as a mediator of cell stress response for both GBM TIC maintenance and GBM progression, independently on the genomic background (proneural or mesenchymal subtype and the mutational state of the main GBM driver genes).

MATERIALS AND METHODS

Study design

To investigate the efficacy of LSD1-dircted therapy for GBM management, we exploited human patient-derived GBM TICs, orthotopic GBM PDXs, and the LSD1i DDP_38003 as the pharmacological strategy to unravel LSD1 role. Animal size sample was chosen to be at least three mice as the minimum number to assess significance basing on preliminary data. Animals were randomized and evaluated by two blinded operators. Biological replicates are described in each figure legend.

Cell culture

GBM TICs from human GBM specimen were grown as spheroid aggregates (*63*). Information for each patient-derived TIC culture is provided in table S2. Details for GBM TIC maintenance are reported in the Supplementary Materials.

Chemicals and low-glutamine experiments

LSD1i was administered as specified for each experiment. To induce stress, GBM TICs were treated with either l-histidinol (2 mM, HisOH; Merck Life Science, #H6647), thapsigargin (2.5 µM; Merck Life Science, #T903), or tunicamycin (2 µM; Merck Life Science, #T7765). For the low-glutamine experiments, GBM TICs were cultured in Dulbecco's modified Eagle's medium/F12 medium containing the indicated concentrations of glutamine: standard concentration (2 mM; SG) and low concentration (0.5 mM; LG).

GBM TIC infection

LSD1 silencing was achieved by means of MISSIONpLKO.1-puro Empty Vector Plasmid DNA (Sigma-Aldrich) harboring either the sequence targeting human *LSD1* (TRCN0000046071; here sh71) or a nontargeting short hairpin RNA (shRNA) (SHC002; here shNT). Pinco-GFP-

ΔN-LSD1^{WT} or Pinco-GFP-ΔN-LSD1^{K661A} [gift from S.M., European Institute of Oncology (IEO), Milan] has been exploited to overexpress an N-terminal truncated (172 to 833) form of LSD1 WT (Δ*N-LSD1*^{WT}) and LSD1 catalytic mutant (Δ*N-LSD1*^{K661A}) in LSD1-KO GBM TICs. GBM TICs expressing ATF4 cDNA were generated by lentiviral infection using lentiviral particles (TLO1001 - Lenti-hCMV-ORF-IRES-bsd, transOMIC) harboring human *ATF4* cDNA. Empty lentiviral particles were used as controls. Blasticidin-resistant cells were selected for 10 days. Lentiviral particles targeting human *CBP* (TRCN0000006485) and MISSION TurboGFP shRNA Control Transduction Particles (Sigma-Aldrich) were used to silence CBP expression in GBM TICs. Cells were selected with puromycin for 72 hours. pLentiLox3.7 vector encoding Luc2 cDNA (gift from L. Lanfrancone, IEO, Milan) was exploited to obtain GBM TICs expressing firefly luciferase. After puromycin selection, cells were seeded in limiting dilution conditions to obtain a single sphere. *Luc2*high-expressing spheres were then identified after incubation with luciferin (150 µg/ml) in phosphate-buffered saline (PBS) and luminescence analyses using PerkinElmer's IVIS Lumina Series III instrument. Lentivirus packaging and transduction were performed as previously described (*63*).

Measure of the ATF4 transcriptional rate

In the bidirectional pSMALB-ATF4 lentiviral reporter vector (gift from P. Pelicci, IEO, Milan), mRNA expression correlates between blue fluorescent protein (*BFP*) and *ATF4-GFP*. GBM TICs were marked by either BFP as a readout of transduction or GFP as a measure of the *ATF4* mRNA translation rate. After GBM TIC infection, BFP fluorescence was measured using FACS Vantage SE FACSCanto II flow cytometer (BD Biosciences). *ATF4* promoter activity was calculated as the transgene ratio between GFP and BFP (TGR = GFP mean fluorescence intensity/TagBFP mean fluorescence intensity).

ChIP and ChIP-seq analyses

Detailed protocols for ChIP are given in the Supplementary Materials. The antibodies used for ChIP-seq are anti-LSD1 (10 µg; Abcam, Ab17721), anti-ATF4 (10 µg; Merck Life Science, ABE387), anti-H3K4me1 (1 µg; Abcam, Ab8895), anti-H3K4me2 (1 µg; Abcam, Ab32356), and anti-H3K4me3 (1 µg; Abcam, Ab8580). DNA libraries were prepared by the Genomic Unit (IEO).

Mice

Female CD1-nude mice (4 to 6 weeks old) were obtained from Charles River Laboratories (Charles River). All animal procedures were approved by the OPBA (Organismo per il Benessere e Protezione Animale) of the Cogentech animal facility. The project has been approved by the Italian Ministry of Health (Authorization 556/2016-PR). Animal experiments were performed in accordance with the Italian laws (D.L.vo 116/92 and following additions), which enforce EU 86/609 Directive. Mice were housed at the Cogentech animal facility according to the guidelines set out in Commission Recommendation 2007/526/EC, 18 June 2007. GBM TICs (10^5) were resuspended in 2 µl of PBS and stereotaxically injected into the mice nucleus caudatus (coordinates from bregma: 1 mm posterior, 3 mm left lateral, and 3.5 mm in depth) (*63*). Tumor-bearing mice were monitored daily to evaluate tumor progression, and those losing more than 20% of the body weight, exhibiting signs of

morbidity, and/or development of neurological symptoms were sacrificed. For LSD1i experiments, mice were treated with LSD1i (17 mg/kg) or vehicle (40% polyethylene glycol 400 and 5% glucose) twice per week for 4 weeks by oral gavage, starting from 2 weeks after GBM TIC injection.

Statistical analyses

For cell culture experiments, three biological replicates have been performed, and each condition was tested in triplicate, unless otherwise specified. For in vivo experiments, the *n* values are specified in each legend. Statistical analyses are indicated in the figure legends and were calculated using the software GraphPad Prism. Student's *t* test and Mann-Whitney test were used to compare two groups. For quantification with more than two groups, one-way analysis of variance (ANOVA) analysis followed by Kruskal-Wallis test was used. The correlations were calculated by linear regression (Pearson's *r*). The survival curves were tested with log-rank test.

Acknowledgments

We thank F. DiMeco, at Istituto Neurologico "Carlo Besta," Milan, for patient samples for histology; M. Patane' at Istituto Neurologico Carlo Besta, Milan, for histopathology on human GBM specimens; L. Rizzuti at IEO, Milan, for ATAC-seq; D. Capello at the University of Piemonte Orientale, Novara, for intellectual discussion; and IEO Technological Units, Mouse Genetics Service, and qPCR Service at Cogentech for technical assistance.
Funding: This work was supported by grants to G.P. from the Italian Association for Cancer Research (AIRC, IG-2017-20140) and the Italian Ministry of Health (Ricerca Finalizzata, RF-2016-02361429).
Author contributions: S.F., D.O., B.C., and G.M. conducted the experiments and analyzed the data. E.C. and D.C. performed the bioinformatic analysis. C.R. performed animal experiments. M.R.F. and L.F. performed PLA experiments. R.N. performed hPTMs analyses. L.N. performed MS experiments. T.B. guided the proteomic study. M.Q., L.B., R.B., and B.P. contributed to immunohistochemistry experiments. S.B. and C.M. performed CETSA experiments. C.M. and M.V. provided DDP_38003 and oversaw LSD1i in vivo administration. S.G. provided bioinformatic support. C.M., M.V., T.B., and G.P. provided critical competencies. S.F., D.O., and G.P. designed the experiments, interpreted the results, wrote the manuscript, and prepared the figures. G.P. supervised the entire work. All the authors revised and approved the manuscript.
Competing interests: The authors declare that they have no competing interests.

REFERENCES

1. D. N. Louis, A. Perry, G. Reifenberger, A. vonDeimling, D. Figarella-Branger, W. K. Cavenee, H. Ohgaki, O. D. Wiestler, P. Kleihues, D. W. Ellison, The 2016 World Health Organization classification of tumors of the central nervous system: A summary. Acta Neuropathol. 131, 803–820 (2016).
2. R. Stupp, W. P. Mason, M. J. VanDen Bent, M. Weller, B. Fisher, M. J. B. Taphoorn, K. Belanger, A. A. Brandes, C. Marosi, U. Bogdahn, J. Curschmann, R. C. Janzer, S. K. Ludwin, T. Gorlia, A. Allgeier, D. Lacombe, J. G. Cairncross, E. Eisenhauer, R. O. Mirimanoff, Radiotherapy plus concomitant and adjuvant temozolomide for glioblastoma. N. Engl. J. Med. 352, 987–996 (2005).
3. R. G. W. Verhaak, K. A. Hoadley, E. Purdom, V. Wang, Y. Qi, M. D. Wilkerson, C. R. Miller, L. Ding, T. Golub, J. P. Mesirov, G. Alexe, M. Lawrence, M. O'Kelly, P. Tamayo, B. A. Weir, S. Gabriel, W. Winckler, S. Gupta, L. Jakkula, H. S. Feiler, J. G. Hodgson, C. D. James, J. N. Sarkaria, C. Brennan, A. Kahn, P. T. Spellman, R. K. Wilson, T. P. Speed, J. W. Gray, M. Meyerson, G. Getz, C. M. Perou, D. N. Hayes; Cancer Genome atlas Research Network, Integrated genomic analysis identifies clinically relevant subtypes of glioblastoma characterized by abnormalities in PDGFRA, IDH1, EGFR, and NF1. Cancer Cell 17, 98–110 (2010).
4. D. Beier, J. B. Schulz, C. P. Beier, Chemoresistance of glioblastoma cancer stem cells- much more complex than expected. Mol. Cancer 10, 128 (2011).
5. M. Mannino, A. J. Chalmers, Radioresistance of glioma stem cells: Intrinsic characteristic or property of the 'microenvironment-stem cell unit'? Mol. Oncol. 5, 374–386 (2011).
6. R. Galli, E. Binda, U. Orfanelli, B. Cipelletti, A. Gritti, S. De Vitis, R. Fiocco, C. Foroni, F. Dimeco, A. Vescovi, Isolation and characterization of tumorigenic, stem-like neural precursors from human glioblastoma. Cancer Res. 64, 7011–7021 (2004).
7. B. C. Prager, S. Bhargava, V. Mahadev, C. G. Hubert, J. N. Rich, Glioblastoma stem cells: Driving resilience through chaos. Trends Cancer 6, 223–235 (2020).
8. M. C. Cabrera, Cancer stem cell plasticity and tumor hierarchy. World J. Stem Cells 7, 27–36 (2015).
9. A. Dirkse, A. Golebiewska, T. Buder, P. V. Nazarov, A. Muller, S. Poovathingal, N. H. C. Brons, S. Leite, N. Sauvageot, D. Sarkisjan, M. Seyfrid, S. Fritah, D. Stieber, A. Michelucci, F. Hertel, C. Herold-Mende, F. Azuaje, A. Skupin, R. Bjerkvig, A. Deutsch, A. Voss-Böhme, S. P. Niclou, Stem cell-associated heterogeneity in glioblastoma results from intrinsic tumor plasticity shaped by the microenvironment. Nat. Commun.
10, 1787 (2019). 10. A. Barski, S. Cuddapah, K. Cui, T. Y. Roh, D. E. Schones, Z. Wang, G. Wei, I. Chepelev, K. Zhao, High-resolution profiling of histone methylations in the human genome. Cell 129, 823–837 (2007).
11. Y. Shi, F. Lan, C. Matson, P. Mulligan, J. R. Whetstine, P. A. Cole, R. A. Casero, Y. Shi, Histone demethylation mediated by the nuclear amine oxidase homolog LSD1. Cell 119, 941–953 (2004).
12. E. Metzger, M. Wissmann, N. Yin, J. M. Müller, R. Schneider, A. H. F. M. Peters, T. Günther, R. Buettner, R. Schüle, LSD1 demethylates repressive histone marks to promote androgen-receptor-dependent transcription. Nature 437, 436–439 (2005).
13. B. Majello, F. Gorini, C. Saccà, S. Amente, Expanding the role of the histone lysine-specific demethylase LSD1 in cancer. Cancers 11, 324 (2019).

14. A. Maiques-Diaz, T. C. P. Somervaille, LSD1: Biologic roles and therapeutic targeting. Epigenomics 8, 1103–1116 (2016).
15. J. Wang, S. Hevi, J. K. Kurash, H. Lei, F. Gay, J. Bajko, H. Su, W. Sun, H. Chang, G. Xu, F. Gaudet, E. Li, T. Chen, The lysine demethylase LSD1 (KDM1) is required for maintenance of global DNA methylation. Nat. Genet. 41, 125–129 (2009).
16. P. Karakaidos, J. Verigos, A. Magklara, Lsd1/kdm1a, a gate-keeper of cancer stemness and a promising therapeutic target. Cancers 11, 1821 (2019). 17. M. M. Singh, B. Johnson, A. Venkatarayan, E. R. Flores, J. Zhang, X. Su, M. Barton, F. Lang, J. Chandra, Preclinical activity of combined HDAC and KDM1A inhibition in glioblastoma. Neuro Oncol.
17, 1463–1473 (2015).
18. D. Kozono, J. Li, M. Nitta, O. Sampetrean, D. Gonda, D. S. Kushwaha, D. Merzon, V. Ramakrishnan, S. Zhu, K. Zhu, H. Matsui, O. Harismendy, W. Hua, Y. Mao, C.-H. Kwon, H. Saya, I. Nakano, D. P. Pizzo, S. R. VandenBerg, C. C. Chen, Dynamic epigenetic regulation of glioblastoma tumorigenicity through LSD1 modulation of MYC expression. Proc. Natl. Acad. Sci. 112, E4055–E4064 (2015).
19. G. R. Sareddy, S. Viswanadhapalli, P. Surapaneni, T. Suzuki, A. Brenner, R. K. Vadlamudi, Novel KDM1A inhibitors induce differentiation and apoptosis of glioma stem cells via unfolded protein response pathway. Oncogene 36, 2423–2434 (2017).
20. J. Wang, F. Lu, Q. Ren, H. Sun, Z. Xu, R. Lan, Y. Liu, D. Ward, J. Quan, T. Ye, H. Zhang, Novel histone demethylase LSD1 inhibitors selectively target cancer cells with pluripotent stem cell properties. Cancer Res. 71, 7238–7249 (2011).
21. Y. Fang, G. Liao, B. Yu, LSD1/KDM1A inhibitors in clinical trials: Advances and prospects. J. Hematol. Oncol. 12, 129 (2019).
22. C. Richichi, D. Osti, M. Del Bene, L. Fornasari, M. Patanè, B. Pollo, F. DiMeco, G. Pelicci, Tumor-initiating cell frequency is relevant for glioblastoma aggressiveness. Oncotarget 7, 71491–71503 (2016).
23. P. Vianello, O. A. Botrugno, A. Cappa, R. Dal Zuffo, P. Dessanti, A. Mai, B. Marrocco, A. Mattevi, G. Meroni, S. Minucci, G. Stazi, F. Thaler, P. Trifiró, S. Valente, M. Villa, M. Varasi, C. Mercurio, Discovery of a novel inhibitor of histone lysine-specific demethylase 1A (KDM1A/LSD1) as orally active antitumor agent. J. Med. Chem. 59, 1501–1517 (2016).
24. R. Ravasio, E. Ceccacci, L. Nicosia, A. Hosseini, P. L. Rossi, I. Barozzi, L. Fornasari, R. D. Zuffo, S. Valente, R. Fioravanti, C. Mercurio, M. Varasi, A. Mattevi, A. Mai, G. Pavesi, T. Bonaldi, S. Minucci, Targeting the scaffolding role of LSD1 (KDM1A) poises acute myeloid leukemia cells for retinoic acid–induced differentiation. Sci. Adv. 6, eaax2746 (2020).
25. C. P. Couturier, S. Ayyadhury, P. U. Le, J. Nadaf, J. Monlong, G. Riva, R. Allache, S. Baig, X. Yan, M. Bourgey, C. Lee, Y. C. D. Wang, V. Wee Yong, M. C. Guiot, H. Najafabadi, B. Misic, J. Antel, G. Bourque, J. Ragoussis, K. Petrecca, Single-cell RNA-seq reveals that glioblastoma recapitulates a normal neurodevelopmental hierarchy. Nat. Commun. 11, 3406 (2020).
26. P. Brescia, C. Richichi, G. Pelicci, Current strategies for identification of glioma stem cells: Adequate or unsatisfactory? J. Oncol. 2012, 1–10 (2012).
27. I. M. N. Wortel, L. T. van der Meer, M. S. Kilberg, F. N. van Leeuwen, Surviving stress: Modulation of ATF4-mediated stress responses in normal and malignant cells. Trends Endocrinol. Metab. 28, 794–806 (2017).
28. N. Ohoka, S. Yoshii, T. Hattori, K. Onozaki, H. Hayashi, TRB3, a novel ER stress-inducible gene, is induced via ATF4-CHOP pathway and is involved in cell death. EMBO J. 24, 1243–1255 (2005).

29. C. Jousse, C. Deval, A. C. Maurin, L. Parry, Y. Chérasse, C. Chaveroux, R. Lefloch, P. Lenormand, A. Bruhat, P. Fafournoux, TRB3 inhibits the transcriptional activation ofstress-regulated genes by a negative feedback on the ATF4 pathway. J. Biol. Chem. 282, 15851–15861 (2007).
30. P. Van Galen, A. Kreso, N. Mbong, D. G. Kent, T. Fitzmaurice, J. E. Chambers, S. Xie, E. Laurenti, K. Hermans, K. Eppert, S. J. Marciniak, J. C. Goodall, A. R. Green, B. G. Wouters, E. Wienholds, J. E. Dick, The unfolded protein response governs integrity of the haematopoietic stem-cell pool during stress. Nature 510, 268–272 (2014).
31. T. B. Rogers, G. Inesi, R. Wade, W. J. Lederer, Use of thapsigargin to study Ca2+ homeostasis in cardiac cells. Biosci. Rep. 15, 341–349 (1995).
32. P. Zhang, B. C. McGrath, J. Reinert, D. S. Olsen, L. Lei, S. Gill, S. A. Wek, K. M. Vattem, R. C. Wek, S. R. Kimball, L. S. Jefferson, D. R. Cavener, The GCN2 eIF2α kinase is required for adaptation to amino acid deprivation in mice. Mol. Cell. Biol. 22, 6681–6688 (2002).
33. H. P. Harding, Y. Zhang, H. Zeng, I. Novoa, P. D. Lu, M. Calfon, N. Sadri, C. Yun, B. Popko, R. Paules, D. F. Stojdl, J. C. Bell, T. Hettmann, J. M. Leiden, D. Ron, An integrated stress response regulates amino acid metabolism and resistance to oxidative stress. Mol. Cell 11, 619–633 (2003).
34. A. Maiques-Diaz, G. J. Spencer, J. T. Lynch, F. Ciceri, E. L. Williams, F. M. R. Amaral, D. H. Wiseman, W. J. Harris, Y. Li, S. Sahoo, J. R. Hitchin, D. P. Mould, E. E. Fairweather, B. Waszkowycz, A. M. Jordan, D. L. Smith, T. C. P. Somervaille, Enhancer activation by pharmacologic displacement of LSD1 from GFI1 induces differentiation in acute myeloid leukemia. Cell Rep. 22, 3641–3659 (2018).
35. A. Sehrawat, L. Gao, Y. Wang, A. Bankhead, S. K. McWeeney, C.J. King, J. Schwartzman, J. Urrutia, W. H. Bisson, D.J. Coleman, S. K.Joshi, D.-H. Kim, D. A. Sampson, S. Weinmann, B. V. S. Kallakury, D. L. Berry, R. Haque, S. K. VanDen Eeden, S. Sharma, J. Bearss, T. M. Beer, G. V. Thomas, L. M. Heiser, J.J. Alumkal, LSD1 activates a lethal prostate cancer gene network independently ofits demethylase function. Proc. Natl. Acad. Sci. 115, E4179–E4188 (2018).
36. Y. J. Shi, C. Matson, F. Lan, S. Iwase, T. Baba, Y. Shi, Regulation of LSD1 histone demethylase activity by its associated factors. Mol. Cell 19, 857–864 (2005).
37. C. C. Sze, A. Shilatifard, MLL3/MLL4/COMPASS family on epigenetic regulation of enhancer function and cancer. Cold Spring Harb. Perspect. Med. 6, a026427 (2016).
38. H. M. Chan, N. B. La Thangue, p300/CBP proteins: HATs for transcriptional bridges and scaffolds. J. Cell Sci. 114, 2363–2373 (2001).
39. F. Gachon, G. Gaudray, S. Thébault, J. Basbous, J. A. Koffi, C. Devaux, J. M. Mesnard, The cAMP response element binding protein-2 (CREB-2) can interact with the C/EBPhomologous protein (CHOP). FEBS Lett. 502, 57–62 (2001).
40. F. Gachon, C. Devaux, J. M. Mesnard, Activation of HTLV-I transcription in the presence of Tax is independent of the acetylation of CREB-2 (ATF-4). Virology 299, 271–278 (2002).
41. H.-C. Tsai, H. Li, L. Van Neste, Y. Cai, C. Robert, F. V. Rassool, J. J. Shin, K. M. Harbom, R. Beaty, E. Pappou, J. Harris, R.-W. C. Yen, N. Ahuja, M. V. Brock, V. Stearns, D. Feller-Kopman, L. B. Yarmus, Y.-C. Lin, A. L. Welm, J.-P. Issa, I. Minn, W. Matsui, Y.-Y. Jang, S. J. Sharkis, S. B. Baylin, C. A. Zahnow, Transient low doses ofDNA-demethylating agents exert durable antitumor effects on hematological and epithelial tumor cells. Cancer Cell 21, 430–446 (2012).
42. D. H. Lee, H. W. Ryu, H. R. Won, S. H. Kwon, Advances in epigenetic glioblastoma therapy. Oncotarget 8, 18577–18589 (2017).

43. M. M. Singh, C. A. Manton, K. P. Bhat, W. W. Tsai, K. Aldape, M. C. Barton, J. Chandra, Inhibition of LSD1 sensitizes glioblastoma cells to histone deacetylase inhibitors. Neuro Oncol. 13, 894–903 (2011).
44. M. L. Suvà, E. Rheinbay, S. M. Gillespie, A. P. Patel, H. Wakimoto, S. D. Rabkin, N. Riggi, A. S. Chi, D. P. Cahill, B. V. Nahed, W. T. Curry, R. L. Martuza, M. N. Rivera, N. Rossetti, S. Kasif, S. Beik, S. Kadri, I. Tirosh, I. Wortman, A. K. Shalek, O. Rozenblatt-Rosen, A. Regev, D. N. Louis, B. E. Bernstein, Reconstructing and reprogramming the tumor-propagating potential of glioblastoma stem-like cells. Cell 157, 580–594 (2014).
45. D. Chen, Z. Fan, M. Rauh, M. Buchfelder, I. Y. Eyupoglu, N. Savaskan, ATF4 promotes angiogenesis and neuronal cell death and confers ferroptosis in a xCT-dependent manner. Oncogene 36, 5593–5608 (2017).
46. I. N. Mungrue, J. Pagnon, O. Kohannim, P. S. Gargalovic, A. J. Lusis, CHAC1/MGC4504 is a novel proapoptotic component of the unfolded protein response, downstream of the ATF4-ATF3-CHOP cascade. J. Immunol. 182, 466–476 (2009).
47. W. Rozpedek, D. Pytel, B. Mucha, H. Leszczynska, J. A. Diehl, I. Majsterek, The role of the PERK/eIF2α/ATF4/CHOP signaling pathway in tumor progression during endoplasmic reticulum stress. Curr. Mol. Med. 16, 533–544 (2016).
48. Z. Liu, Q. Shi, X. Song, Y. Wang, Y. Wang, E. Song, Y. Song, Activating transcription factor 4 (ATF4)-ATF3-C/EBP homologous protein (CHOP) cascade shows anessential role intheER stress-induced sensitization oftetrachlorobenzoquinone-challenged PC12 cells toROS-mediated apoptosis via death receptor 5 (DR5) signaling. Chem. Res. Toxicol. 29, 1510–1518 (2016).
49. G. Gargiulo, M. Cesaroni, M. Serresi, N. de Vries, D. Hulsman, S. W. Bruggeman, C. Lancini, M. van Lohuizen, In vivo RNAi screen for BMI1 targets identifies TGF-β/BMP-ER stress pathways as key regulators of neural- and malignant glioma-stem cell homeostasis. Cancer Cell 23, 660–676 (2013).
50. K. Stock, J. Kumar, M. Synowitz, S. Petrosino, R. Imperatore, E. S. J. Smith, P. Wend, B. Purfürst, U. A. Nuber, U. Gurok, V. Matyash, J. H. Wälzlein, S. R. Chirasani, G. Dittmar, B. F. Cravatt, S. Momma, G. R. Lewin, A. Ligresti, L. De Petrocellis, L. Cristino, V. Di Marzo, H. Kettenmann, R. Glass, Neural precursor cells induce cell death of high-grade astrocytomas through stimulation of TRPV1. Nat. Med. 18, 1232–1238 (2012).
51. S. Dey, T. D. Baird, D. Zhou, L. R. Palam, D. F. Spandau, R. C. Wek, Both transcriptional regulation and translational control of ATF4 are central to the integrated stress response. J. Biol. Chem. 285, 33165–33174 (2010).
52. E. Zhao, J. Ding, Y. Xia, M. Liu, B. Ye, J. H. Choi, C. Yan, Z. Dong, S. Huang, Y. Zha, L. Yang, H. Cui, H. F. Ding, KDM4C and ATF4 cooperate in transcriptional control of amino acid metabolism. Cell Rep. 14, 506–519 (2016).
53. D. M. Gwinn, A. G. Lee, M. Briones-Martin-Del-Campo, C. S. Conn, D. R. Simpson, A. I. Scott, A. Le, T. M. Cowan, D. Ruggero, E. A. Sweet-Cordero, Oncogenic KRAS regulates amino acid homeostasis and asparagine biosynthesis via ATF4 and alters sensitivity to l-asparaginase. Cancer Cell 33, 91–107.e6 (2018).
54. I. Nagasawa, M. Koido, Y. Tani, S. Tsukahara, K. Kunimasa, A. Tomida, Disrupting ATF4 expression mechanisms provides an effective strategy for BRAF-targeted melanoma therapy. iScience 23, 101028 (2020).
55. N. M. Peñaranda-Fajardo, C. Meijer, Y. Liang, B. M. Dijkstra, R. Aguirre-Gamboa, W. F. A. den Dunnen, F. A. E. Kruyt, ER stress and UPR activation in glioblastoma: Identification of a

noncanonical PERK mechanism regulating GBM stem cells through SOX2 modulation. Cell Death Dis. 10, 690 (2019).
56. S. Takagi, Y. Ishikawa, A. Mizutani, S. Iwasaki, S. Matsumoto, Y. Kamada, T. Nomura, K. Nakamura, LSD1 inhibitor T-3775440 inhibits SCLC cell proliferation by disrupting LSD1 interactions with SNAG domain proteins INSM1 and GFI1B. Cancer Res. 77, 4652–4662 (2017).
57. H. Lan, M. Tan, Q. Zhang, F. Yang, S. Wang, H. Li, X. Xiong, Y. Sun, LSD1 destabilizes FBXW7 and abrogates FBXW7 functions independent of its demethylase activity. Proc. Natl. Acad. Sci. U.S.A. 116, 12311–12320 (2019).
58. P. Stavropoulos, G. Blobel, A. Hoelz, Crystal structure and mechanism of human lysine-specific demethylase-1. Nat. Struct. Mol. Biol. 13, 626–632 (2006).
59. S. A. Kim, J. Zhu, N. Yennawar, P. Eek, S. Tan, Crystal structure of the LSD1/CoREST histone demethylase bound to its nucleosome substrate. Mol. Cell 78, 903–914.e4 (2020).
60. Y. Chen, J. Kim, R. Zhang, X. Yang, Y. Zhang, J. Fang, Z. Chen, L. Teng, X. Chen, H. Ge, P. Atadja, E. Li, T. Chen, W. Qi, Histone demethylase LSD1 promotes adipocyte differentiation through repressing Wnt signaling. Cell Chem. Biol. 23, 1228–1240 (2016).
61. M. Huang, C. Chen, J. Geng, D. Han, T. Wang, T. Xie, L. Wang, Y. Wang, C. Wang, Z. Lei, X. Chu, Targeting KDM1A attenuates Wnt/β-catenin signaling pathway to eliminate sorafenib-resistant stem-like cells in hepatocellular carcinoma. Cancer Lett. 398, 12–21 (2017).
62. W. Tao, A. Zhang, K. Zhai, Z. Huang, H. Huang, W. Zhou, Q. Huang, X. Fang, B. C. Prager, X. Wang, Q. Wu, A. E. Sloan, M. S. Ahluwalia, J. D. Lathia, J. S. Yu, J. N. Rich, S. Bao, SATB2 drives glioblastoma growth by recruiting CBP to promote FOXM1 expression in glioma stem cells. EMBO Mol. Med. 12, e12291 (2020).
63. B. Ortensi, D. Osti, S. Pellegatta, F. Pisati, P. Brescia, L. Fornasari, D. Levi, P. Gaetani, P. Colombo, A. Ferri, S. Nicolis, G. Finocchiaro, G. Pelicci, Rai is a new regulator of neural progenitor migration and glioblastoma invasion. Stem Cells 30, 817–832 (2012).
64. Y. Perez-Riverol, A. Csordas, J. Bai, M. Bernal-Llinares, S. Hewapathirana, D. J. Kundu, A. Inuganti, J. Griss, G. Mayer, M. Eisenacher, E. Pérez, J. Uszkoreit, J. Pfeuffer, T. Sachsenberg, Ş. Yilmaz, S. Tiwary, J. Cox, E. Audain, M. Walzer, A. F. Jarnuczak, T. Ternent, A. Brazma, J. A. Vizcaíno, The PRIDE database and related tools and resources in 2019: Improving support for quantification data. Nucleic Acids Res. 47, D442–D450 (2019).
65. Y. Hu, G. K. Smyth, ELDA: Extreme limiting dilution analysis for comparing depleted and enriched populations in stem cell and other assays. J. Immunol. Methods 347, 70–78 (2009).
66. A. A. Borisy, P. J. Elliott, N. W. Hurst, M. S. Lee, J. Lehár, E. R. Price, G. Serbedzija, G. R. Zimmermann, M. A. Foley, B. R. Stockwellt, C. T. Keith, Systematic discovery of multicomponent therapeutics. Proc. Natl. Acad. Sci. U.S.A. 100, 7977–7982 (2003).
67. A. Dobin, C. A. Davis, F. Schlesinger, J. Drenkow, C. Zaleski, S. Jha, P. Batut, M. Chaisson, T. R. Gingeras, STAR: Ultrafast universal RNA-seq aligner. Bioinformatics 29, 15–21 (2013).
68. Y. Liao, G. K. Smyth, W. Shi, FeatureCounts: An efficient general purpose program for assigning sequence reads to genomic features. Bioinformatics 30, 923–930 (2014).
69. M. D. Robinson, D. J. McCarthy, G. K. Smyth, edgeR: A bioconductor package for differential expression analysis of digital gene expression data. Bioinformatics 26, 139–140 (2009).
70. S. Picelli, A. K. Björklund, B. Reinius, S. Sagasser, G. Winberg, R. Sandberg, Tn5 transposase and tagmentation procedures for massively scaled sequencing projects. Genome Res. 24, 2033–2040 (2014).

71. R. Noberini, C. Restellini, E. O. Savoia, T. Bonaldi, Enrichment of histones from patient samples for mass spectrometry-based analysis of post-translational modifications. Methods 184, 19–28 (2020).
72. R.Noberini, R. Longuespée, C. Richichi, G. Pruneri, M. Kriegsmann, G. Pelicci, T. Bonaldi, PAT-H-MS coupled withlaser microdissection tostudy histone post-translational modifications inselected cell populations from pathology samples. Clin. Epigenetics 9, 69 (2017).
73. R. Noberini, D. Osti, C. Miccolo, C. Richichi, M. Lupia, G. Corleone, S.-P. Hong, P. Colombo, B. Pollo, L. Fornasari, G. Pruneri, L. Magnani, U. Cavallaro, S. Chiocca, S. Minucci, G. Pelicci, T. Bonaldi, Extensive and systematic rewiring of histone post-translational modifications in cancer model systems. Nucleic Acids Res. 46, 3817–3832 (2018).
74. J. Cox, N. Neuhauser, A. Michalski, R. A. Scheltema, J. V. Olsen, M. Mann, Andromeda: A peptide search engine integrated into the MaxQuant environment. J. Proteome Res. 10, 1794–1805 (2011).

Fig. 1. LSD1 pharmacological inhibition has therapeutic potential prolonging the survival of GBM PDXs.

(**A**) Representative images of LSD1 expression patterns in human GBMs. Scale bars, 200 µm. (**B**) LSD1 protein by Western blot in human GBM TICs from different patients. NPCs were used as nontumoral counterpart. Under the Western blot, the densitometric quantification of LSD1 signals is reported: Proteins are normalized on actin and are expressed as fold change relative to NPCs. (**C**) Representative confocal images of GBM TICs stained for LSD1 (red) and DNA (blue). Scale bar, 20 µm. DAPI, 4',6-diamidino-2-phenylindole. (**D**) CETSA thermal melt profiles showing LSD1i's (17 mg/kg) ability to bind LSD1 within the brain (T_{agg}, aggregation temperature) ($P = 0.0009$). (**E**) H3K4me2 in normal (filled circles) and tumor (empty circles) tissues from the brain of mice treated with vehicle ($n = 12$) or LSD1i ($n = 6$), as quantified by MS. The histogram shows L/H ratios, where L is the sample and H is the internal standard. LSD1i- and vehicle-treated samples were compared by Student's *t* test. *$P < 0.05$. (**F** and **G**) Survival curve (vehicle, $n = 22$ and LSD1i, $n = 22$; $P = 0.001$, log-rank test) (F) and tumor incidence (G) of LSD1i- or vehicle-treated GBM#22 PDXs. (**H** and **I**) Survival curve (vehicle, $n = 16$ and LSD1i, $n = 18$; $P < 0.001$, log-rank test) (H) and representative bioluminescence images (I) of LSD1i- or vehicle-treated mice transplanted with the luciferase-positive GBM#18 TICs. Luciferase signals were acquired 1 and 6 weeks after LSD1i treatment start. (**J**) LSD1i EC_{50} calculation for the indicated GBM TICs and NPCs treated with LSD1i or vehicle for 7 days. (**K** and **L**) Growth (K) and caspase 3/7 activity (L) of the indicated GBM TICs treated with or without LSD1i (LSD1i: 2.5 µM for GBM#22 and GBM#7 TICs and 5 µM for GBM#18 TICs). (**M**) Neurosphere formation efficiency of the indicated GBM TICs treated with or without 2.5 µM LSD1i. Sphere formation ability was evaluated after two serial platings. (K to M) Results show one representative experiment, expressed as means ± SD ($n = 3$ independent replicates; two-tailed Student's *t* test, *$P <$ 0.05, **$P < 0.0$
1, and ***$P < 0.001$). FC, fold change.

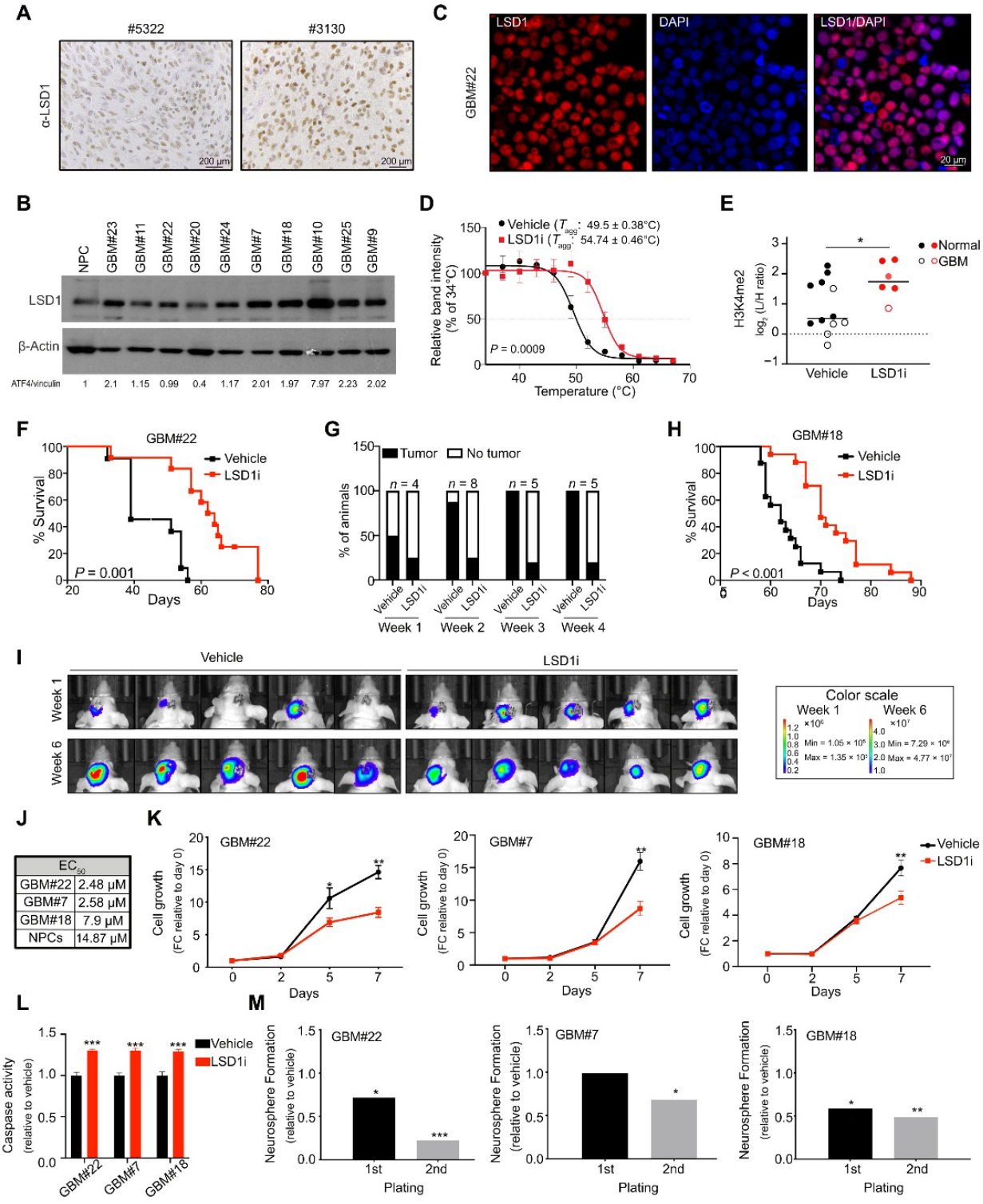
A
#5322
#3130
α-LSD1
200 μm
C
LSD1
DAPI
LSD1/DAPI
GBM#22
20 μm
B
NPC
GBM#23
GBM#11
GBM#22
GBM#20
GBM#24
GBM#7
GBM#18
GBM#10
GBM#25
GBM#9
LSD1
β-Actin
ATF4/vinculin 1 2.1 1.15 0.99 0.4 1.17 2.01 1.97 7.97 2.23 2.02
D
Vehicle (T_{agg}: 49.5 ± 0.38°C)
LSD1i (T_{agg}: 54.74 ± 0.46°C)
Relative band intensity (% of 34°C)
P = 0.0009
Temperature (°C)
E
Normal
GBM
H3K4me2 log2 (L/H ratio)
Vehicle
LSD1i
F
GBM#22
Vehicle
LSD1i
% Survival
P = 0.001
Days
G
Tumor
No tumor
% of animals
n = 4
n = 8
n = 5
n = 5
Vehicle
LSD1i
Week 1
Week 2
Week 3
Week 4
H
GBM#18
Vehicle
LSD1i
% Survival
P < 0.001
Days
I
Vehicle
LSD1i
Week 1
Week 6
Color scale
Week 1
Week 6
Min = 1.05 × 10⁵
Max = 1.35 × 10⁶
Min = 7.29 × 10⁶
Max = 4.77 × 10⁷
J
EC50
GBM#22 2.48 μM
GBM#7 2.58 μM
GBM#18 7.9 μM
NPCs 14.87 μM
K
GBM#22
GBM#7
GBM#18
Vehicle
LSD1i
Cell growth (FC relative to day 0)
Days
L
Caspase activity (relative to vehicle)
Vehicle
LSD1i
GBM#22
GBM#7
GBM#18
M
GBM#22
GBM#7
GBM#18
Neurosphere Formation (relative to vehicle)
1st
2nd
Plating

Fig. 2. LSD1 genetic targeting mirrors LSD1 pharmacological inhibition in GBM TICs.

(**A**) Growth of LSD1-KO GBM TICs (KO#1 and KO#2) compared to their control. LSD1 expression of the indicated samples as assessed by Western blot is shown (top). (**B**) Neurosphere formation efficiency of the indicated LSD1-KO (KO#1 and KO#2) relative to control GBM TICs. Sphere formation ability was evaluated after two serial platings. (**C**) Survival curves ($P = 0.001$, log-rank test) of mice transplanted with the indicated LSD1-KO (KO#1, $n = 7$ and KO#2, $n = 8$) and control GBM#22 ($n = 10$). (**D**) In vivo estimated stem cell frequency for the indicated LSD1-KO and control cells [Extreme limiting dilution assay (ELDA) algorithm] ($n = 3$ for each group). (**E**) Growth of LSD1-silenced (sh71) GBM TICs from different patients (GBM#22, GBM#7, and GBM#18) compared to their nontargeting control (shNT). LSD1 expression of the indicated samples as assessed by Western blot is shown (top). (**F**) Caspase 3/7 activity of the indicated samples upon LSD1 silencing. (**G** and **H**) Neurosphere formation efficiency (G) and in vitro limiting dilution assays (H) of the indicated samples upon LSD1 silencing. (**I**) Survival curves of mice injected with LSD1-silenced and control GBM TICs ($n = 5$ for each group). Results from two representative samples (GBM#22, $P = 0.005$; GBM#18, $P < 0.001$, log-rank test) are shown. (**J**) In vivo estimated stem cell frequency for the indicated LSD1-silenced and control cells (ELDA algorithm) ($n = 3$ for each group). (A, B, and D to F) Results show one representative experiment, expressed as means ± SD ($n = 3$ independent replicates; two-tailed Student's t test, $^{*}P < 0.05$, $^{**}P < 0.01$, and $^{***}P < 0.001$).

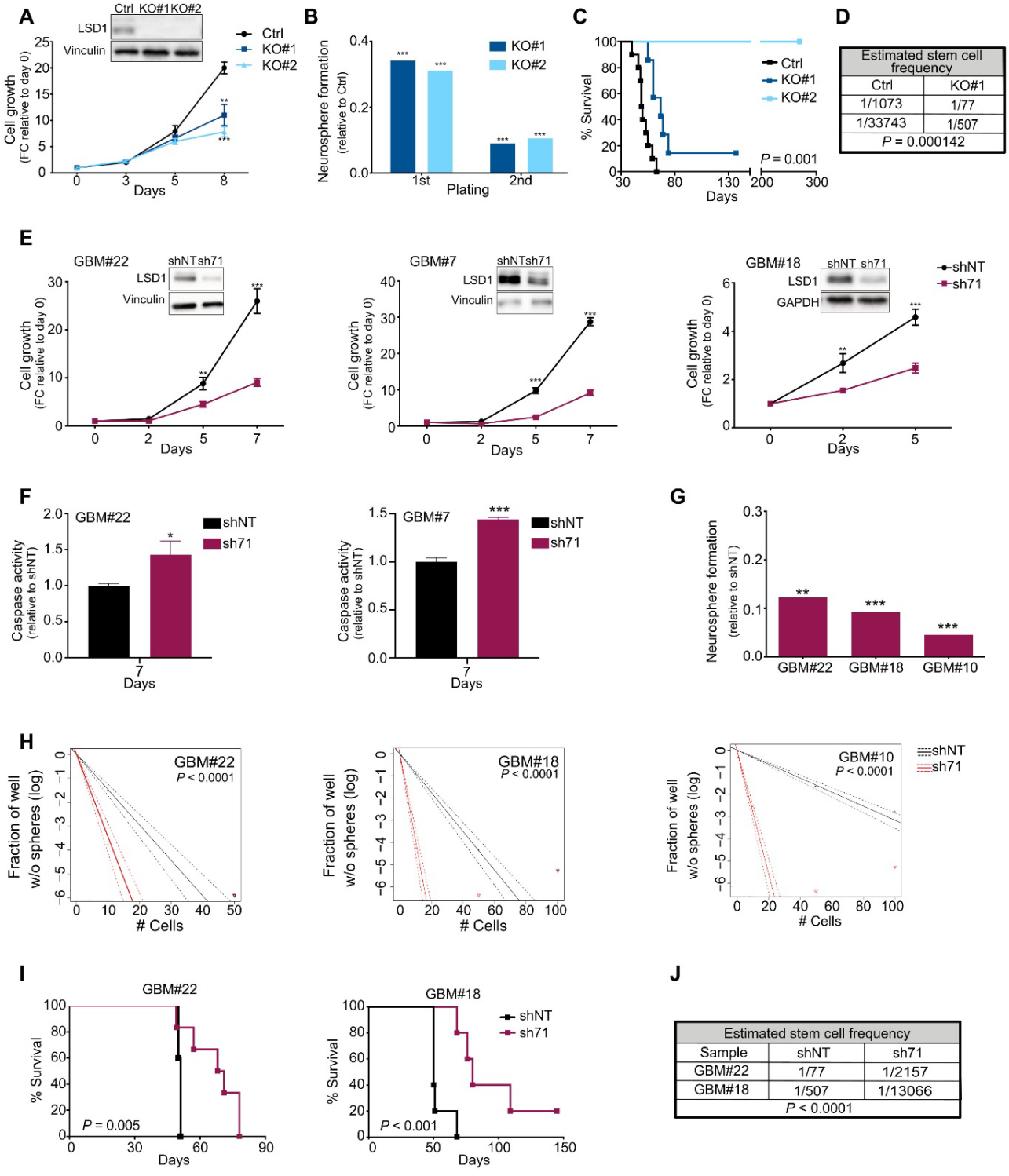
A
Ctrl KO#1 KO#2
LSD1
Vinculin
Cell growth (FC relative to day 0)
Days
Ctrl
KO#1
KO#2
B
Neurosphere formation (relative to Ctrl)
KO#1
KO#2
1st
2nd
Plating
C
% Survival
Ctrl
KO#1
KO#2
P = 0.001
Days
D
Estimated stem cell frequency
Ctrl | KO#1
1/1073 | 1/77
1/33743 | 1/507
P = 0.000142
E
GBM#22
GBM#7
GBM#18
shNT sh71
LSD1
Vinculin
GAPDH
Cell growth (FC relative to day 0)
Days
shNT
sh71
F
GBM#22
GBM#7
Caspase activity (relative to shNT)
shNT
sh71
Days
G
Neurosphere formation (relative to shNT)
GBM#22
GBM#18
GBM#10
H
GBM#22
GBM#18
GBM#10
P < 0.0001
Fraction of well w/o spheres (log)
Cells
shNT
sh71
I
GBM#22
GBM#18
% Survival
P = 0.005
P < 0.001
Days
shNT
sh71
J
Estimated stem cell frequency
Sample | shNT | sh71
GBM#22 | 1/77 | 1/2157
GBM#18 | 1/507 | 1/13066
P < 0.0001

Fig. 3. LSD1 targeting affects ATF4-mediated ISR in GBM TICs.

(**A**) Heatmap showing DEGs in LSD1-silenced (sh71) and control (shNT) GBM#22 TICs, as assessed by RNA-seq (FDR ≤ 0.05). Data from two biological replicates are shown. RPKM, Reads Per Kilobase of exon per Million mapped reads. (**B**) GO analysis based on the DEGs showed in (A). (**C**) GSEA enrichment score curves of LSD1-silenced (sh71) and control (shNT) GBM#22 TICs. ES, enrichment score; NES, normalized enrichment score. (**D**) Upstream regulator predicted analysis based on the DEGs showed in (A). (**E**) ATF4 expression by qRT-PCR upon LSD1 silencing (sh71) in GBM TICs from different patients (GBM#22, GBM#7, GBM#10, and GBM#18). (**F**) ATF4 promoter activity in LSD1-silenced (sh71) and control (shNT) GBM TICs. Error bars represent means ± SD (*n* = 2 independent replicates; two-tailed Student's *t* test, **P* < 0.05). (**G** and **H**) ISR signaling by Western blot in LSD1-silenced (sh71) and control (shNT) GBM#22 TICs upon thapsigargin (G) or l-histidinol treatment (H). Under the Western blot, the densitometric quantification of ATF4 signals is reported: Proteins are normalized on vinculin and are expressed as fold change relative to untreated shNT cells. (**I**) ATF4 target gene expression by qRT-PCR in LSD1-silenced (sh71) and control (shNT) GBM#22 TICs. (E and I) Results show one representative experiment, expressed as means ± SD (*n* = 3 independent replicates; two-tailed Student's *t* test, **P* < 0.05, ***P* < 0.01, and ****P* < 0.001).

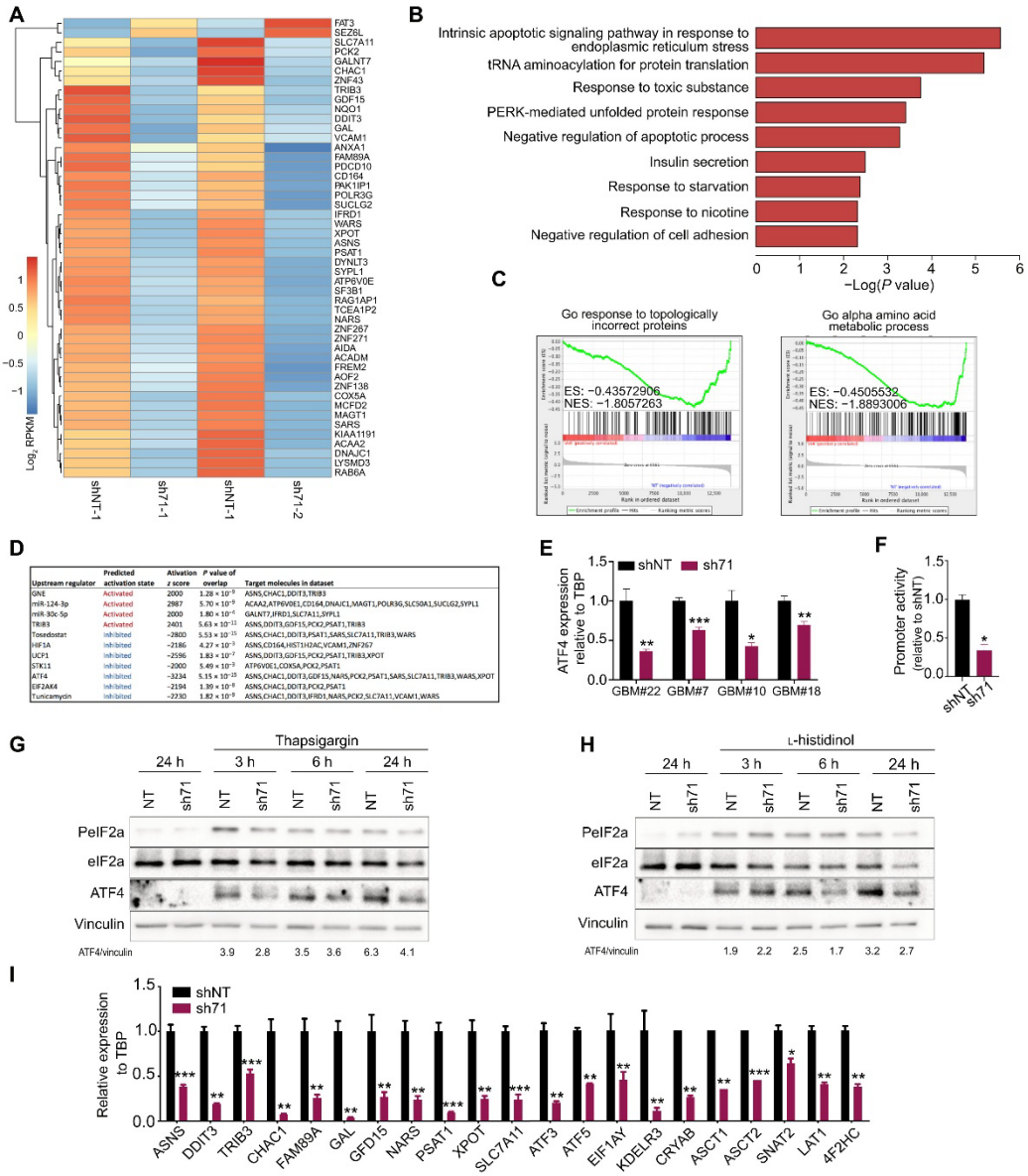

Fig. 4. LSD1 targeting affects ATF4-mediated ISR in GBM TICs.

(**A**) LSD1 and ATF4 expression by Western blot in LSD1-KO GBM TICs with or without ΔN-LSD1^{WT} overexpression. Mock-transduced (empty) LSD1-KO GBM TICs were used as a control. Data are representative of three similar experiments. Under the Western blot, the densitometric quantification of ATF4 signals is reported: Proteins are normalized on vinculin and are expressed as fold change relative to LSD1-KO empty cells. (**B** and **C**) Growth (B) and neurosphere formation efficiency (C) of LSD1-KO GBM TICs with (KO#1 ΔN-LSD1^{WT}) or without (KO#1 empty) ΔN-LSD1^{WT} overexpression. (**D**) ATF4 and ASNS expression by Western blot in LSD1-silenced (sh71) GBM#22 TICs with (sh71 ATF4) or without (sh71 empty) ATF4 overexpression. Nontargeted mock-transduced GBM#22 TICs (shNT empty) were used as a control. Under Western blot, the densitometric quantification of ATF4 signals is reported: Proteins are normalized on vinculin and are expressed as fold change relative to control cells. (**E** to **G**) Growth (E), caspase 3/7 activity (F), and neurosphere formation efficiency (G) of LSD1-silenced (sh71) GBM TICs with (sh71 ATF4) or without (sh71 empty) ATF4 overexpression. Nontargeted mock-transduced GBM#22 TICs (shNT empty) were used as a control. (**H**) ATF4 target gene expression by qRT-PCR in LSD1-silenced (sh71) GBM#22 TICs with (sh71 ATF4) or without (sh71 empty) ATF4 overexpression. Nontargeted mock-transduced GBM#22 TICs (shNT empty) were used as a control. (B, C, and E to H) Results show one representative experiment, expressed as means ± SD (*n* = 3 independent replicates; two-tailed Student's *t* test, **P* < 0.05, ***P* < 0.01, and ****P* < 0.001).

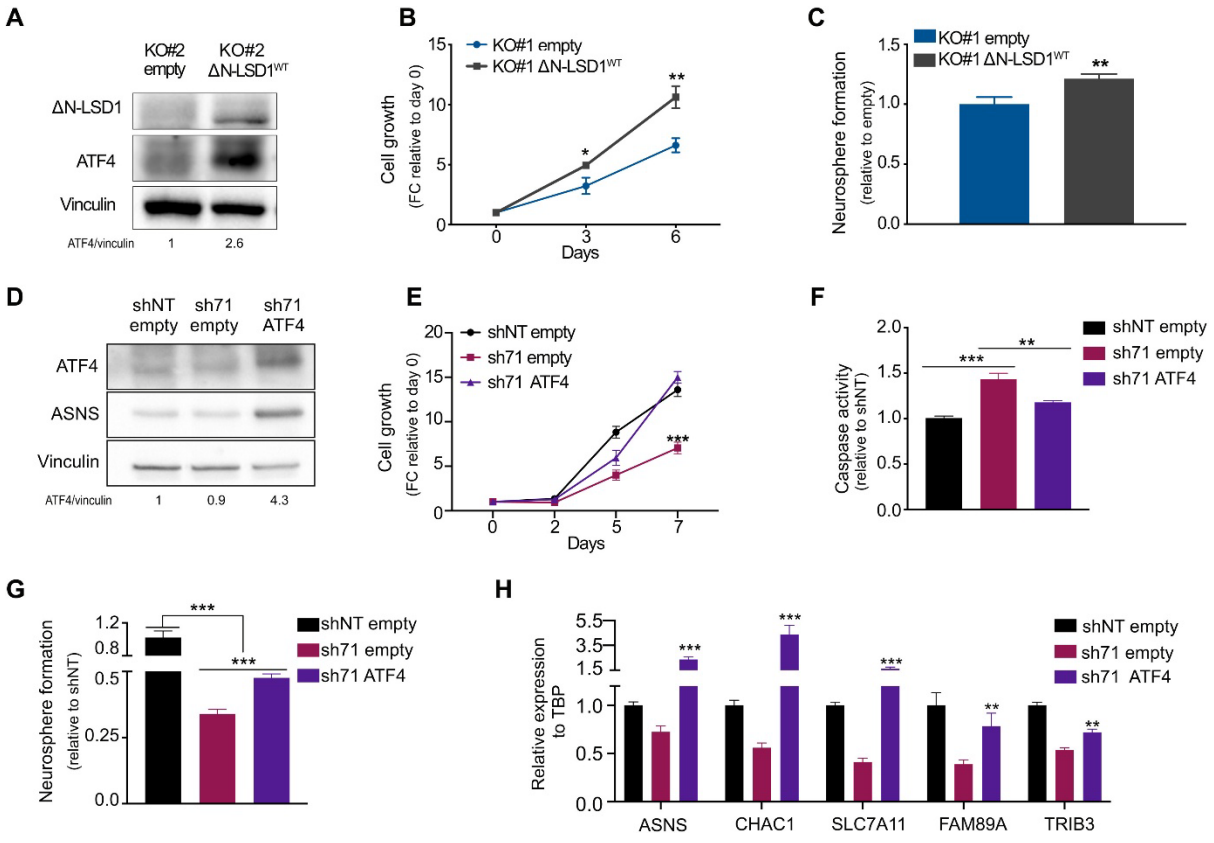

Fig. 5. LSD1 targeting affects ATF4-mediated ISR in GBM TICs.

(**A** to **C**) ISR signaling by Western blot in GBM#22 TICs with or without 2.5 μM LSD1i upon thapsigargin (A), l-histidinol (B), or tunicamycin (C) treatment. Under the Western blot, the densitometric quantification of ATF4 signals is reported: Proteins are normalized on vinculin and are expressed as fold change relative to untreated vehicle cells. Results show a representative experiment (*n* = 2 of 3 independent replicates). (**D**) ATF4 target gene expression by qRT-PCR in GBM#22 TICs with or without 2.5 μM LSD1i, under nonstressed conditions and upon l-histidinol (H) treatment for the indicated time points. LSD1i- and vehicle-treated samples have been compared within each time point. (**E**) Growth of GBM#22 TICs with or without 2.5 μM LSD1i upon thapsigargin (T) (left) or l-histidinol (H) (right) treatment. (**F**) Growth of GBM#22 TICs with or without 2.5 μM LSD1i cultured in standard glutamine (SG) and low-glutamine (LG) medium. (D to F) Results show one representative experiment, expressed as means ± SD (*n* = 3 independent replicates; two-tailed Student's *t* test, **P* < 0.05, ***P* < 0.01, and ****P* < 0.001).

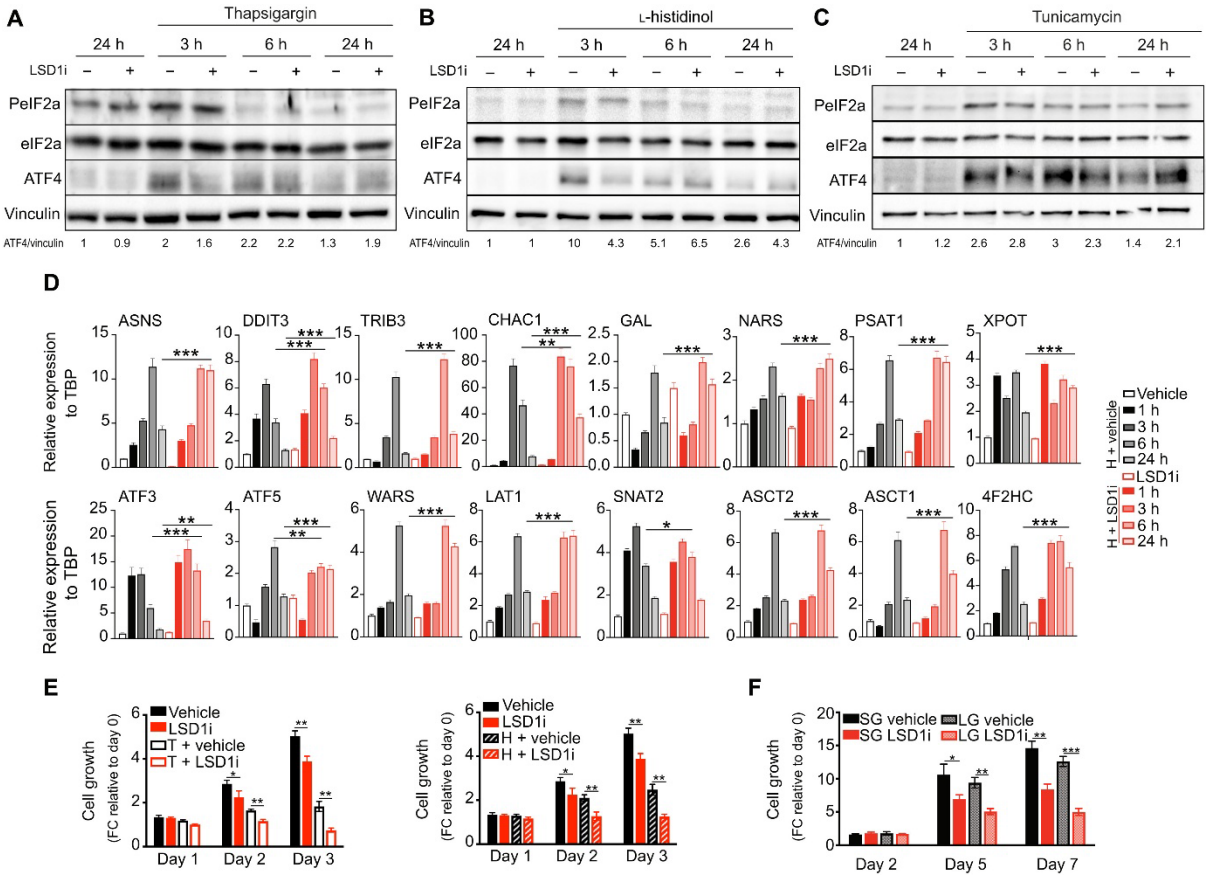

Fig. 6. LSD1 and ATF4 share common DNA binding sites.

(**A**) ChIP-seq signal tracks showing LSD1-binding peak within representative DEGs identified in LSD1 RNA-seq. Tracks are visualized with the University of California Santa Cruz Genome Browser. (**B**) LSD1 ChIP-qPCR at the promoter of the indicated genes. Immunoglobulin G (IgG) and a gene desert region on human chromosome 12 were used as controls. (**C**) ATF4-binding motif enrichment in LSD1-bound DEG promoters (± 2.5 kbp around TSS) (empirical $P = 0.032$). (**D**) LSD1 ChIP-qPCR at the ATF4 promoter. IgG and a gene desert region on human chromosome 12 were used as controls. (**E**) ATF4 ChIP-qPCR at the promoter of the indicated genes. IgG and a gene desert region on human chromosome 12 were used as controls. (**F**) Heatmap showing LSD1 ChIP-seq signals in LSD1i- or vehicle-treated GBM#22 TICs. Common: LSD1 binding sites present in both LSD1i- and vehicle-treated cells. Gain: LSD1 binding sites in LSD1i-treated cells only. Lost: LSD1 binding sites in vehicle-treated cells only. (**G**) List of the 48 DEGs identified in LSD1 RNA-seq and bound by LSD1. Flags indicate the presence or absence of LSD1 peaks at the promoter of the corresponding genes. Black: LSD1-binding peak in vehicle-treated GBM#22 TICs; red: LSD1-binding peak in LSD1i-treated GBM#22 TICs; white: no LSD1 binding. (**H** and **I**) LSD1 (H) and ATF4 (I) ChIP-qPCR at the promoter of the indicated genes in LSD1i- and vehicle-treated GBM#22 TICs. IgG and a gene desert region on human chromosome 12 were used as controls. (**J**) LSD1 and ATF4 expression by Western blot in LSD1-KO GBM TICs overexpressing either ΔN-LSD1^{WT} or ΔN-LSD1^{K661A}. Mock-transduced LSD1-KO GBM TICs (empty) were used as a control. Under the Western blot, the densitometric quantification of ATF4 signals is reported: Proteins are normalized on vinculin and are expressed as fold change relative to LSD1-KO empty cells. (**K** and **L**) Growth (K) and neurosphere formation efficiency (L) of LSD1-KO GBM TICs overexpressing either ΔN-LSD1^{WT} or ΔN-LSD1^{K661A}. (**M**) ATF4 target gene expression by qRT-PCR in LSD1-KO GBM TICs overexpressing either ΔN-LSD1^{WT} or ΔN-LSD1^{K661A}. Mock-transduced LSD1-KO GBM TICs (empty) were used as a control. (K to M) Results show one representative experiment, expressed as means ± SD ($n = 3$ independent replicates; two-tailed Student's t test, $^{*}P < 0.05$, $^{**}P < 0.01$, and $^{***}P < 0.001$).

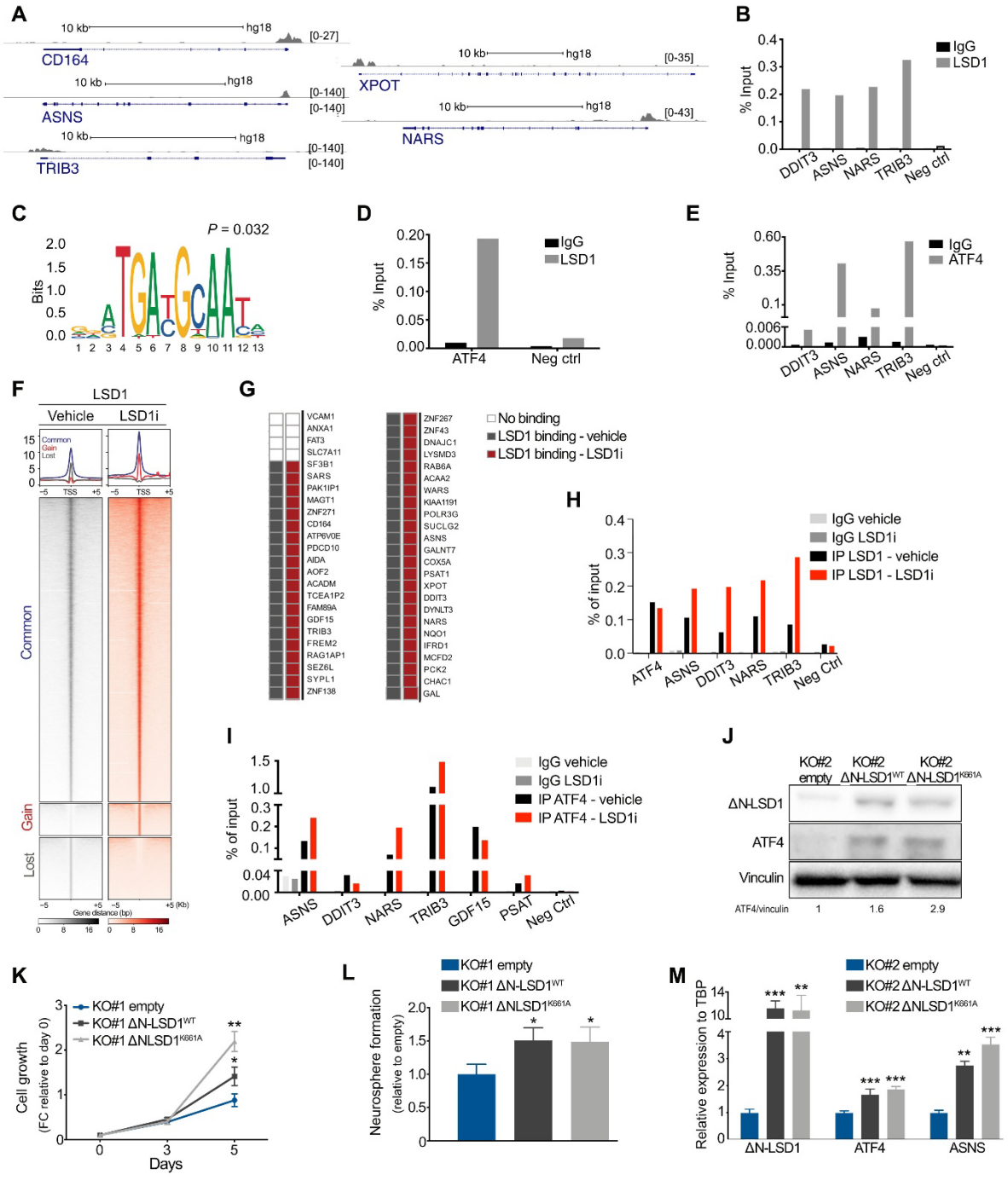
A
10 kb
hg18
[0-27]
CD164
[0-35]
XPOT
[0-140]
ASNS
[0-43]
NARS
TRIB3
B
% Input
IgG
LSD1
DDIT3
ASNS
NARS
TRIB3
Neg ctrl
C
P = 0.032
Bits
D
E
ATF4
F
LSD1
Vehicle
LSD1i
Common
Gain
Lost
TSS
Gene distance (bp)
G
No binding
LSD1 binding - vehicle
LSD1 binding - LSD1i
H
% of input
IgG vehicle
IgG LSD1i
IP LSD1 - vehicle
IP LSD1 - LSD1i
ATF4
Neg Ctrl
I
IP ATF4 - vehicle
IP ATF4 - LSD1i
GDF15
PSAT
J
KO#2 empty
KO#2 ΔN-LSD1WT
KO#2 ΔN-LSD1K661A
ΔN-LSD1
Vinculin
ATF4/vinculin
K
KO#1 empty
KO#1 ΔN-LSD1WT
KO#1 ΔNLSD1K661A
Cell growth
(FC relative to day 0)
Days
L
Neurosphere formation
(relative to empty)
M
Relative expression to TBP

Fig. 7. LSD1i treatment reduces ATF4 activation by modifying LSD1 protein complex in GBM TICs. (**A**) Table of LSD1 complex in GBM#22 TICs. (**B**) Volcano plot of LSD1 protein interactors after LSD1i treatment. Recruited or evicted interactors are shown on the top right quadrant and top left quadrant, respectively. Dashed lines define the threshold used to determine recruited and evicted proteins. Student's *t* test was used for statistical analysis of proteins quantified in at least two of three replicates under control and treated condition. (**C**) LSD1 and CBP interaction in GBM#22 TICs using IF-PLA confocal microscopy. Representative images of CBP (mouse monoclonal, red), LSD1 (rabbit polyclonal, green), and nuclei (blue) have been used to monitor localization (first row: wide-field microscopy, pixel sixe of 162 nm) and proximity (second row: maximum intensity projection of a confocal z-stack, pixel size of 138 nm) by PLA. (**D**) CBP silencing efficiency in GBM#22 TICs is shown (left). ATF4 expression by Western blot in CBP-silenced (shCBP) GBM#22 TICs and corresponding controls (Ctrl) under nonstressed conditions and upon l-histidinol treatment for the indicated time points. Under the Western blot, the densitometric quantification of ATF4 signals is reported: Protein amounts are normalized on vinculin and are expressed as fold change relative to untreated Ctrl cells (right). Under the Western blot, the densitometric quantification of CBP signals is reported: Protein quantities are normalized on vinculin and are expressed as fold change relative to Ctrl cells. (**E**) ATF4 target gene expression by qRT-PCR in CBP-silenced (shCBP) GBM#22 TICs and the corresponding controls (Ctrl) under nonstressed conditions and upon l-histidinol (H) treatment for the indicated time points. shCBP and Ctrl samples have been compared within each time point. (**F**) Growth of control (Ctrl) and CBP-silenced (shCBP) GBM#22 TICs with or without 2.5 μM LSD1i upon l-histidinol (H) treatment. (**G**) Selected ATF4 target gene expression by qRT-PCR in CBP-silenced (shCBP) GBM#22 TICs and the corresponding controls (Ctrl), under nonstressed conditions and upon l-histidinol (H) treatment for the indicated time points. LSD1i- and vehicle-treated samples have been compared within each time point. (E to G) Results show one representative experiment, expressed as means ± SD (*n* = 3 independent replicates; two-tailed Student's *t* test, **P* < 0.05, ***P* < 0.01, and ****P* < 0.001). LFQ, label-free quantitation.

A

Complexes	Adj. *P* value
CtBP	5.05×10^{-9}
BHC110	2.95×10^{-7}
Anti-BHC110	1.04304×10^{-6}
Anti-HDAC2	5.32449×10^{-6}
CtBP core	0.296556×10^{-3}
LSD1	0.442375×10^{-3}
PTIP-HMT	0.714423×10^{-3}
CoREST-HDAC	0.180186×10^{-2}
MLL4	0.010055768
MLL3	0.010055768
BHC	0.029983046
REST-CoREST-mSIN3A	0.049513482

B

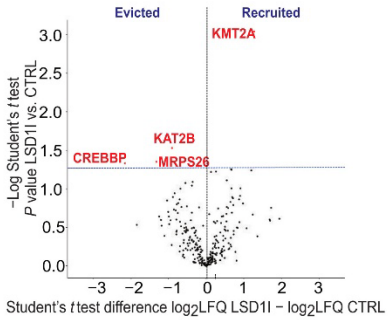

C

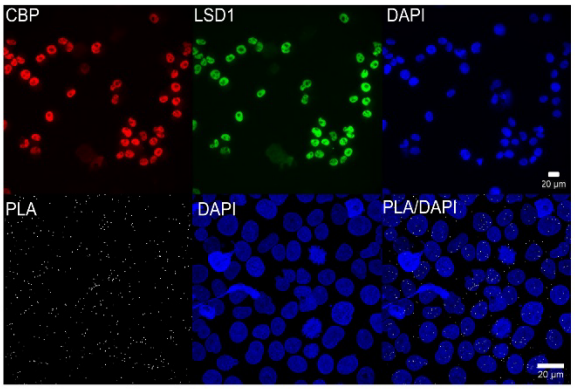

D

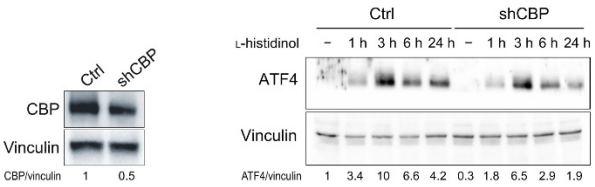

E

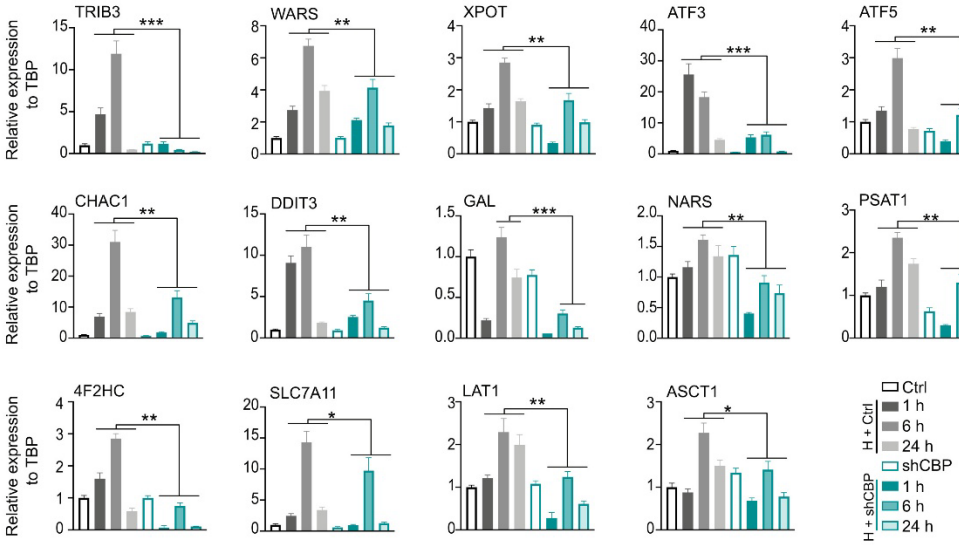

F

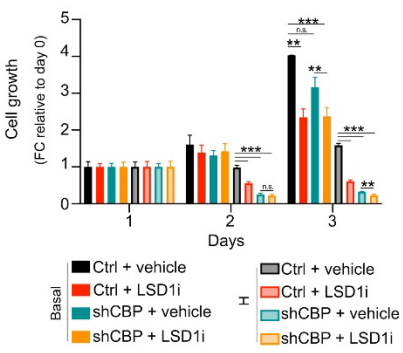

G